A STUDY OF COMPLETE AND INCOMPLETE FUSION IN SOME HEAVY ION INDUCED REACTIONS

DISSERTATION

SUBMITTED IN PARTIAL FULFILLMENT OF THE REQUIREMENTS

FOR THE AWARD OF THE DEGREE OF

Master of Philosophy

IN

Physics

BY

Pushpendra P. Singh

Under the Supervision of

Dr. B. P. Singh

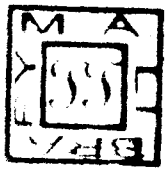

DEPARTMENT OF PHYSICS
ALIGARH MUSLIM UNIVERSITY
ALIGARH (INDIA)

2004

My teachers

(The prime architect of my career)

&

My parents

(The beacon of hope, inspiration, courage and strength)

Dr. B. P. Singh
Reader

Department of Physics
Aligarh Muslim University
Aligarh-202002 (U.P.) INDIA
Phone: (0571) 2701001(Off.)
Fax: (0571) 2701001
E-Mail: *pht06ps1@rediffmail.com*

Certificate

Certified that the work presented in this dissertation is the original work of Mr. Pushpendra P. Singh done under my supervision.

(Dr. B. P. Singh)

Acknowledgments

It is very pleasant for me to utilize this great opportunity to express my sincere indebtedness towards my supervisor, Dr. B. P. Singh for his inspiring guidance, analytical and critical suggestions, constant encouragement and generous support as an intellectual, creative faculty and patience bearer of my mistakes throughout the course of this work.

A specific and respectful acknowledgment is due to my group leader, Prof. R. Prasad for scientific discussions and kind suggestions. He has always been a constant source of inspiration and introducing me to a realistic and solitary picture of experimental nuclear physics.

My special thanks to Dr. Manoj K. Sharma (young scientist, DST) for being available with his comments and suggestions for the improvement of the present work. I thank Ms. Unnati for her immense help in all kinds of computational work. The constant assistance and co-operation, which I received from my colleague Ms. Bhavna Sharma is thankfully acknowledged. I am also thankful to all my friends in general, Mr. Pankaj Kumar (Scientist-C), Ms. Bharti Sharma, Mr. Sudhir Verma, Mr. Vivek Gupta and Ms. Praveena Baghel in particular for their moral support throughout this work.

I am grateful to the Chairman, Department of Physics, for providing all the necessary departmental facilities towards this work.

I thank Prof. Amit Roy, Director, Nuclear Science Center, New Delhi, India for providing necessary facilities for carrying out this work. Thanks are also due to Dr. Sunita Gupta, Dr. H. D. Bhardwaj, Dr. M. M. Musthafa, Mr. Rakesh Kumar, Ms. K. S. Golda, Mr. S. Murlidhar, Mr. N. Madhavan and Dr. R. K. Bhaumik for their valuable help during the experiment.

Last but not least, I am deeply indebted to my family members and relatives especially Er. V. Singh, Suppdt. BR-I (GREF) & Mr. Rajendra K. Singh for their affection and patience and to all those who remembered and wished me on every success with out of their endless strife and blessing it would have been impossible for me to pursue this work.

Pushpendra P. Singh

(Pushpendra P. Singh)

Contents

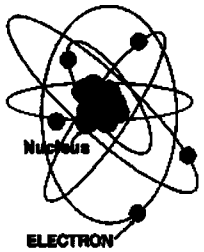

①Introduction

Much of our present knowledge of the structural properties of nuclei is a phenomenal progress of an idea of *'atomism'* in which Anaxgoras, Lecippus and Democritus state that all the matter in the universe is made up of a set of minute, indivisible particles called atom. The British physicist J. J. Thomson, in 1898 conceived the atom as consisting of electrons embedded in a spherical matrix of positive charge[1]. Later, in 1911 E. Rutherford modified it on the basis of large angle α-particle scattering experiment[2]. Results of these experiments indicated that, most of the positive charge and mass of the atom is concentrated in a very small central body called nucleus. The electrons are assumed to revolve in nearly circular orbits about the nucleus and make the atom electrically neutral.

The discovery of natural radioactivity, in 1896, by Henri Becquerel led to contemplate the nature of the nucleus[3]. In 1919, Rutherford achieved the first artificial radioactivity[4, 5]. The nuclear transmutation experiments of Rutherford, Cock-Croft & Walton, I. Curie & Juliet and Fermi suggested new experimental methods to solve basic problems regarding nuclear structure, nuclear properties, nuclear forces, the determination of energy states of nuclei, transition probabilities etc., which opened up a vast field of study of nuclear reactions.

A nuclear reaction occurs when a particular chosen nuclide is bombarded by a projectile of sufficient kinetic energy i.e., the energy of the incident ion must be at least comparable to the Coulomb barrier of the entrance channel. As a consequence, the initial system is transformed into final system, consisting of the products of the reaction i.e., light and/or heavy emitted

particles and residual nucleus followed by the emission of characteristic γ-radiations. Typically, a nuclear reaction may be represented by $X(a,b)Y$. Here, a is the projectile, X is the target nucleus, Y is the residual nucleus and b is the emitted particle.

The nuclear reaction may be broadly categorized as elastic and inelastic nuclear reactions. The elastic nuclear rection is defined to be a collision in which colliding particles change their direction of motion only. In above case, the particles in the exit channel are exactly the same as in the incident channel, with no change in the quantum numbers. While in case of inelastic nuclear reaction, one or both of the interacting partners can change their internal states. In a nuclear reaction, properties of entrance and exit channels are well defined but it is not well understood what exactly happens at the time of interaction of the collision partners. Since the nuclear reaction takes place in a very short time $\approx 10^{-20}$-10^{-16} sec, it can not be visualised directly.

In 1936, N. Bohr proposed the compound nucleus (CN) theory[6] to explain the nuclear reaction mechanism. In CN reaction, the projectile of sufficient kinetic energy interacts with the target nucleus, leading to the formation of quasi-bound intermediate complex system (i.e., the bound configuration of target nucleus and projectile nucleus). The compound nucleus reaction mechanism is considered as a two stage process: the first stage is the capture of projectile by the target forming a composite nucleus and the second stage is the subsequent decay of the composite nucleus. It is further assumed that the total energy of the projectile is shared among all the nucleons of the composite nucleus leading to the establishment of thermodynamic equilibrium.

After a long time sufficient amount of energy may be accumulated on one nucleon or on a group of nucleons to escape. The basic assumption of the CN theory is that the lapse time between formation of the composite nucleus and its decay is too large($\approx 10^{-16}$sec), and no trace is left to decide its mode of formation. In 1950, Ghoshal[7] experimentally verified the validity of Bohr's independent hypothesis. A pictorial representation of the CN formation and decay is shown in Fig.1.1.

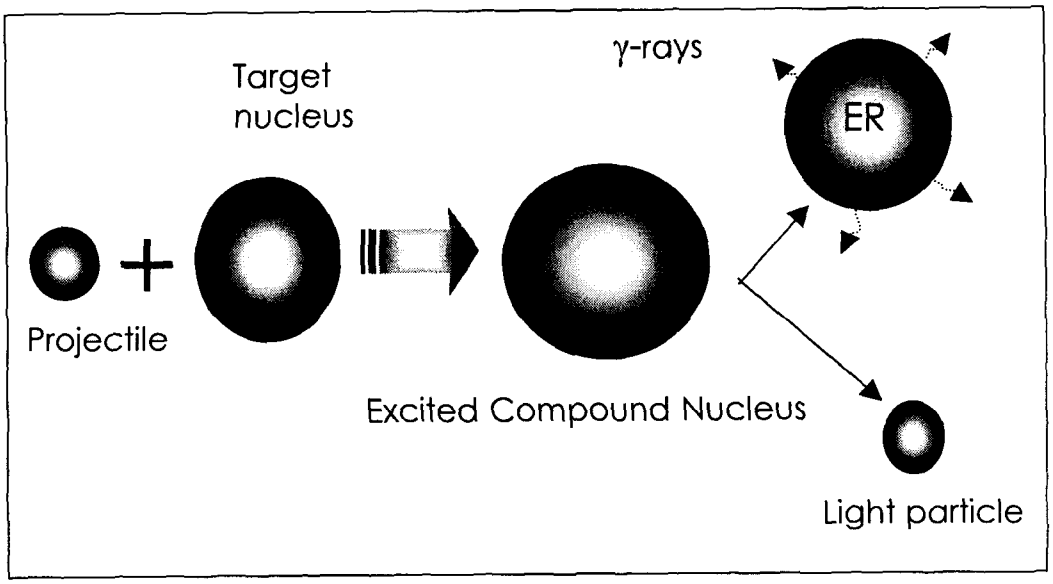

Fig.1.1. Pictorial representation of the CN formation and decay.

On the other hand, the direct reactions occur promptly, on a time scale of the same magnitude as the time it takes for the projectile to traverse the target nucleus(i.e.,$\approx 10^{-22}$sec). Hence, the CN and direct reaction processes

may be distinguised on the basis of interaction time required for the completion of the reaction. The direct reaction may further be classified into two categories as knock-out and stripping/pick-up reactions. In CN reaction the emission of particles/cluster takes place after the esteblishment of thermodynamic equlilibrium. However, it has been inferred from the results of large number of experiments[8, 9, 10] that the emission of particles/clusters may also take place even before the establishment of thermodynamic equilibrium of the compound system. The particles which are emitted before the equilibration of composite system are called pre-equilibrium (PE) particles and the process is referred to as PE or pre-compound reaction mechanism.

Study of nuclear reactions got a big boost with the availability of advanced accelerators and detectors which opened many possibilities for exploring new aspects of nuclear behaviour. With the availability of modern accelerators it has become possible to accelerate heavy ions (from $^{4}_{2}He$ particle, *the lightest heavy ion* to ^{235}U) at energies varying from few MeV/nucleon to many GeV/nucleon. The heavy ion (HI) induced reactions give the possibility to produce complex systems in high spin excited states which do not exist naturally. The accelerator based HI reaction studies started in India in late nineties with the establishment of Pelletron accelerator facilities at the Nuclear Science Center(NSC), New Delhi and the Tata Institute of Fundamental Research(TIFR), Mumbai. The study of heavy ion reactions[11] is quite complicated because both thye projectile and the target are many nucleon systems, having large Coulomb barrier(CB) between the interacting nuclei. The heavy ion reactions are different from light ion induced reactions

in many aspects. The angular momentum of HI's with respect to the center of mass is very large and therefore, it is possible to produce nuclei with high excitation energy and high spin in comparison to that of in case of light ion reactions. Further, the de-Broglie wavelength depends on the mass of the projectile as given in equation(1), hence the projectile of large mass shows very small de-Broglie wavelength,

$$\lambda\!\!\!^{-} = \frac{1}{2\pi}\left[\frac{h^2}{2mE_{lab}}\right]^{1/2} \tag{1}$$

As such the motion of the incident ion may be treated semiclassically. The semi-classical nature of HI reaction makes it possible to give general discription of their classical characteristics, particularly their relative motion along quite well defined orbits in terms of closest distance between interacting nuclei(r_{min}), which is related to the impact parameter(b) as given in equation(2).

$$r_{min} = \frac{b}{\sqrt{[1 - \frac{V(r_{min})}{E_{CM}}]}} \tag{2}$$

where, V(r_{min}) is the nuclear potential acting between the interacting nuclei and E_{CM} is the center of mass energy.

A typical classical picture of heavy ion interaction representing different processes at different impact parameters is shown in Fig.1.2.

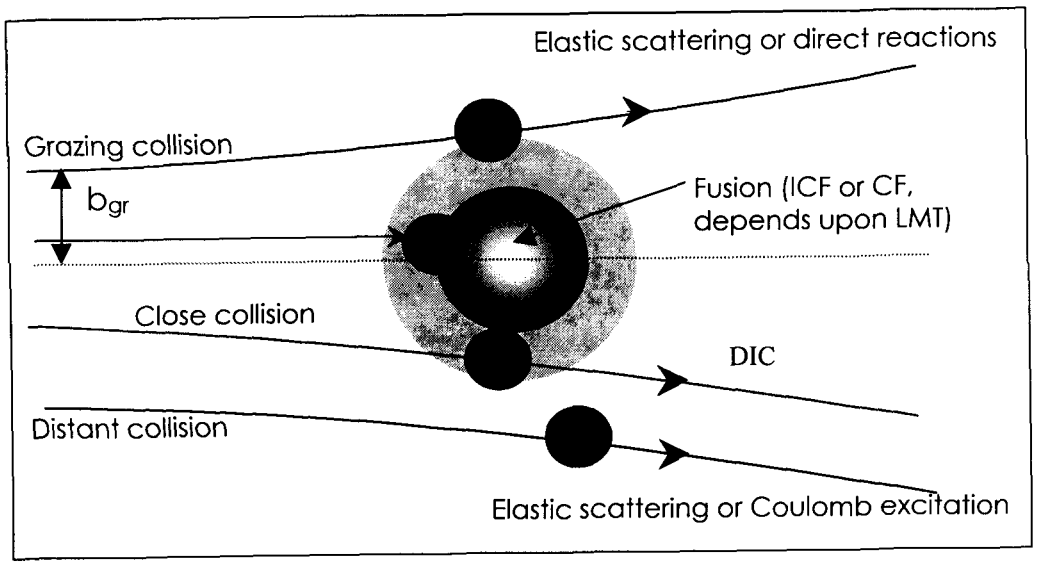

Fig.1.2 Classical picture of Heavy Ion Interaction showing distant collision, grazing collision, close collision and fusion.

At low energies (i.e., below the CB), the projectile interacts only through the Coulomb field at very large impact parameter leading to the *distant collision*. At relatively higher energies the projectile interacts also through the nuclear potential. If the impact parameter (energy dependent) is comperable to the sum of the radii of interacting partners, *grazing collision* takes place and the projectile can be elastically or inelastically scattered. This may lead to one or few nucleon transfer from one nucleus to the other. When the projectile interacts with the target nucleus at relatively high energy just enough to enter in the nuclear range of the interaction of two nuclei then the deep inelastic collision (DIC) dominates. In such a case, the nuclear densities rise very rapidly in the surface region, and few nucleons may get transferred from one nucleus to the other. If the projectile interacts with the target very strongly at still smaller values of impact parameter then it may cause various phenomena like (a) Fusion: so that the both interacting parteners completely

merge into each other leading to the formation of compound nucleus (CN) in excited state which may evaporate nucleons, (b) Fusion-Fission: so that after CN formation at high excitation energy it undergoes fission into two intermediate masses and emitting nucleons. At energies above the Coulomb barrier (CB), it is possible to distinguish the ranges of impact parameters (R_L) and angular momentum (ℓ) which may lead to different type of reactions. This is summerised in Table-1.1

Table-1.1 Ranges of impact parameter and angular momentum associated with different types of heavy-ion interactions

Impact parameter (b)	Angular momentum (ℓ)	Types of interaction
$R_L > R_N$=$(R_1 + R_2)$	$\ell > \ell_N$	Rutherford (Elastic) scattering or Coulomb excitation
$R_L \approx R_N$	$\ell_N > \ell > \ell_{DIC}$	Elastic and inelastic scattering Few-nucleon transfer reactions
$R_L \leq R_N$	$\ell_{DIC} > \ell > \ell_F$	Deep inelastic scattering or close collision
$R_L << R_N$	$\ell < \ell_F$	Fusion

Where, $R_N = R_1 + R_2$ is the sum of radii of interacting partners, R_L= impact parameter. The various reaction types as a function of angular momentum (ℓ) are shown in the Fig.1.3.

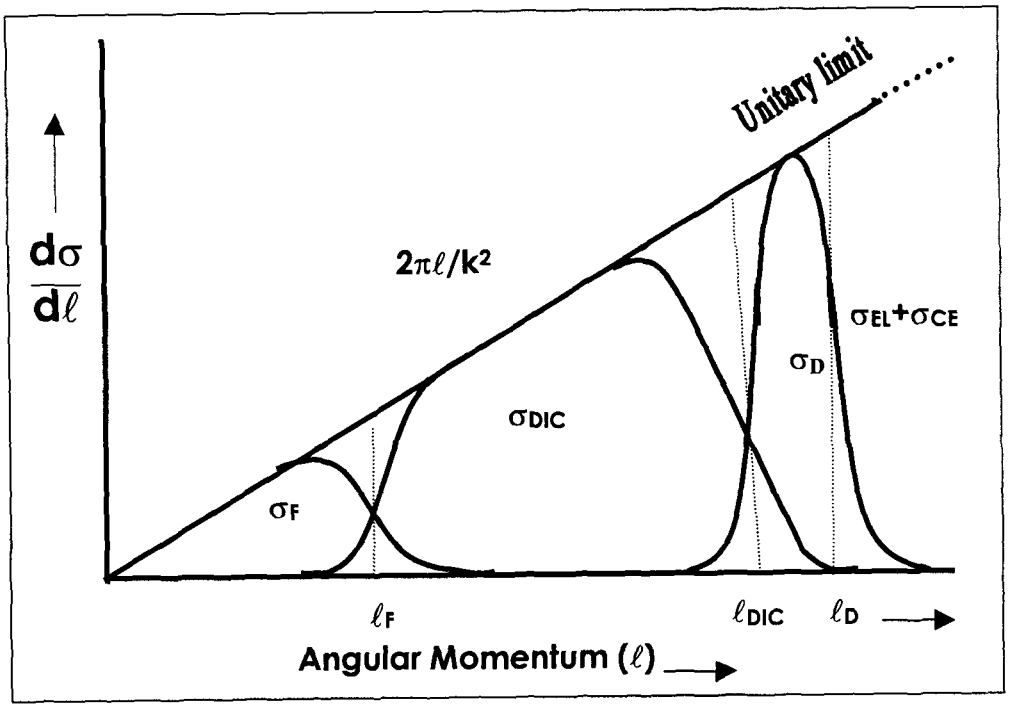

Fig.1.3 Typical graphical representation of different reaction mechanisms as the function of angular momentum (ℓ). The solid line represents the geometricel partial cross-section. The vertical dashed line represent the extension of various (ℓ) windows in a sharp cut off model.

When the center of mass energy of the interacting partners is greater than the barrier height, they overcome the barrier and may loose some of the relative energy leading to the formation of compound nucleus. The partial cross-section for such reaction may be given as,

$$\sigma_\ell^R(E) = \pi\lambda^2(2\ell+1)T_\ell(E) \tag{3}$$

where, $T_\ell(E)$ is the transmission coefficient for the effective potential $V_{eff}(r)$.

The effective potential $V_{eff}(r)$ as a function of distance and relative an-

gular momentum may also be given as,

$$V_{eff}(r) = V_N(r) + V_C(r) + V_{cent}(r) \tag{4}$$

Where; $V_N(r)$ is the strongly attractive nuclear potential, $V_C(r)$ is the repulsive Coulomb potential and $V_{cent}(r)$ is centrifugal potential.

The plots of the $V_{eff}(r)$ effective potential as a function of relative seperation between interacting ions for the different values of ℓ for the system ${}^{16}_{8}O+{}^{169}_{69}Tm$ are given in Fig.1.4.

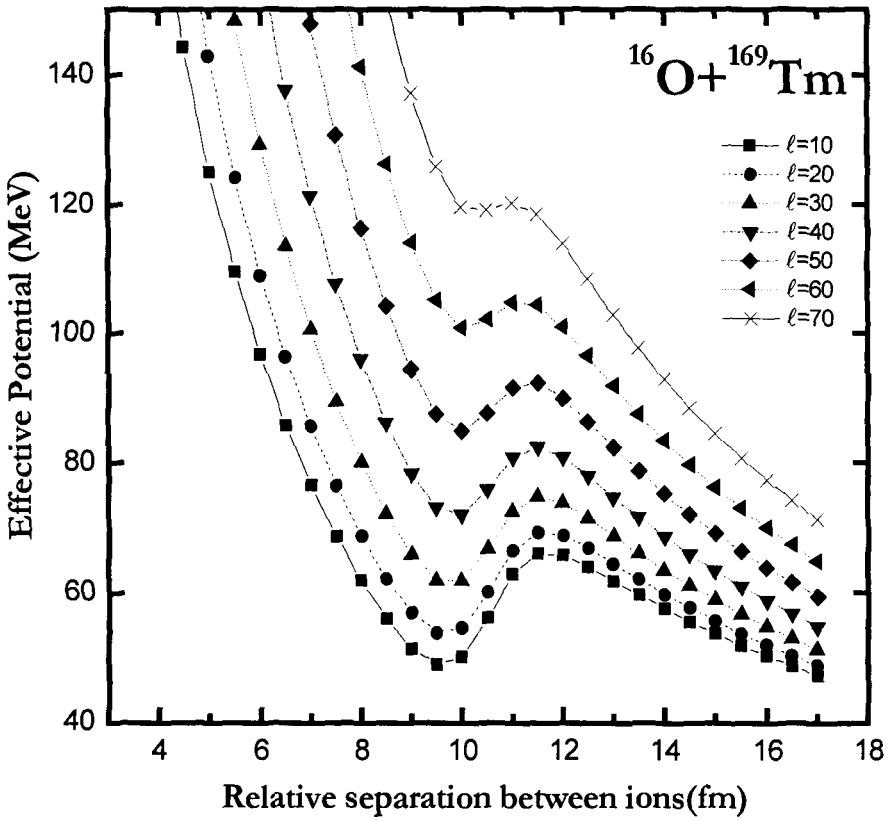

Fig.1.4. Effective potential for ${}^{16}_{8}O+{}^{169}_{69}Tm$ as a function of relative separation between the interacting partners for different values of angular momentum (ℓ).

As mentioned earlier, in HI reactions at energies from near the Coulomb barrier to well above it, different kinds of reaction mechanisms like complete fusion (CF) and incomplete fusion (ICF)compete with each other[12, 13]. In case of CF, whole mass of the projectile fuses with the target nucleus leading to the formation of excited composite system. Here, the total kinetic energy (TKE) and linear momentum of the projectile are shared by all the constituents of the composite system which may decay by emitting nuclear particles and/or characteristic gamma rays. A pictorial representation of CF process is shown in Fig.1.5.

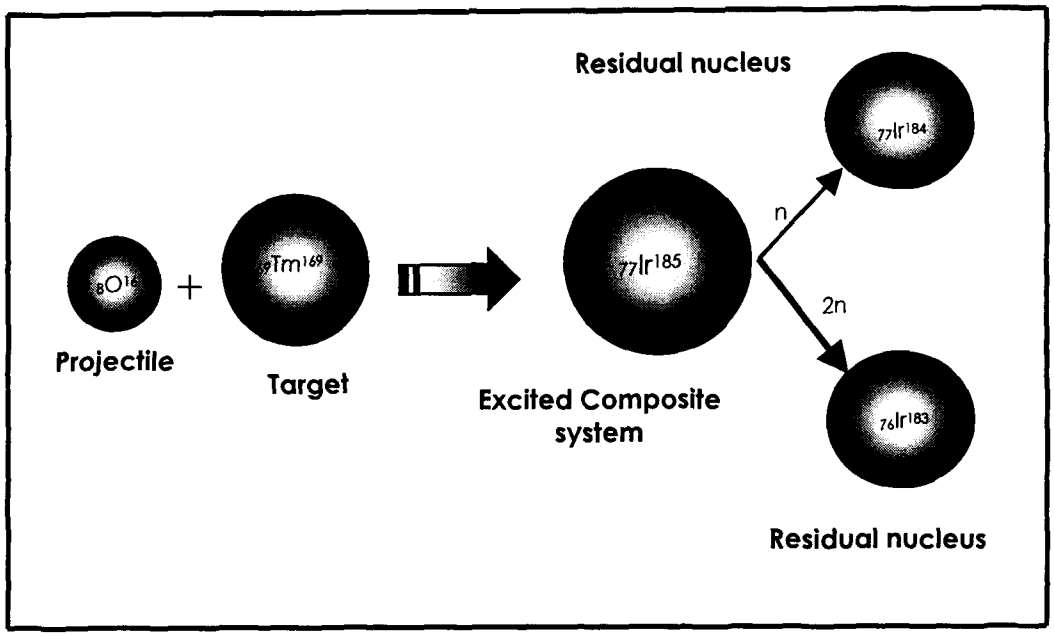

Fig.1.5 Pictorial representation of complete fusion of $^{16}_{8}O$.

In case of ICF, the incident projectile in the presence of nuclear field may break-up into fragments, one of the fragments may fuse with the target nucleus and the remaining part traverses along the beam direction with almost the same velocity as that of incident ion. Depending on the mass of fused fragment partial mometum transfer may take place. Pictorial representation of possible ICF channels for the fusion of different fragments of the $^{16}_{8}O$ projectile are shown in Fig.1.6(a-c).

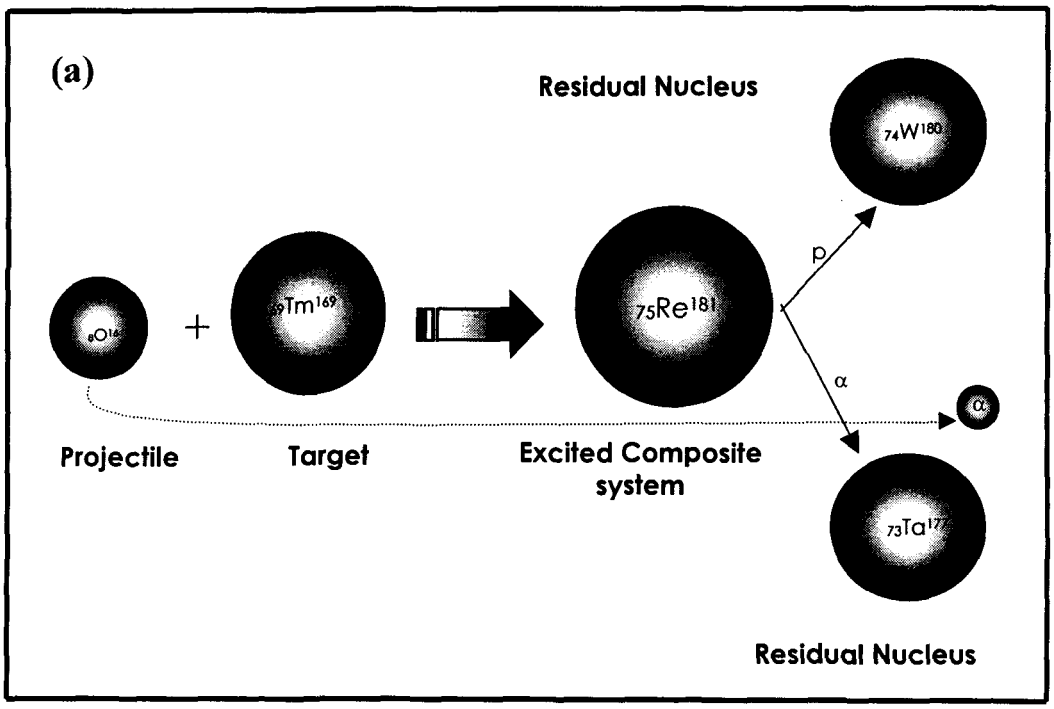

Fig.1.6(a) Pictorial representation of the fusion of 3α particles with the target. .

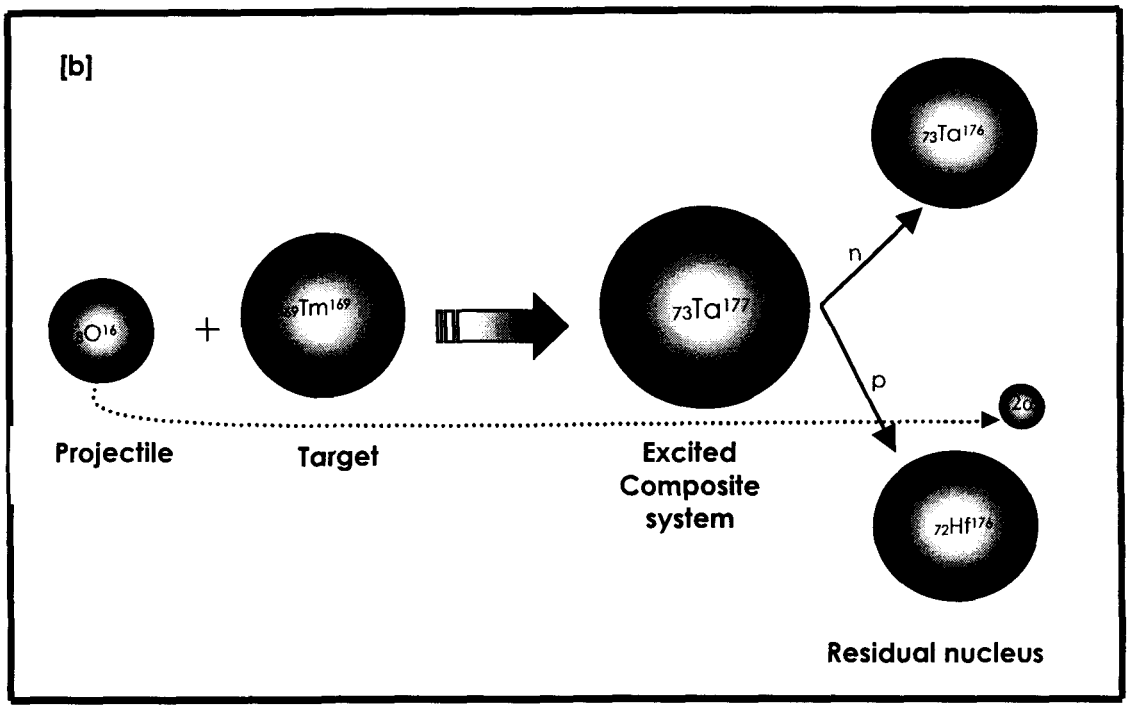

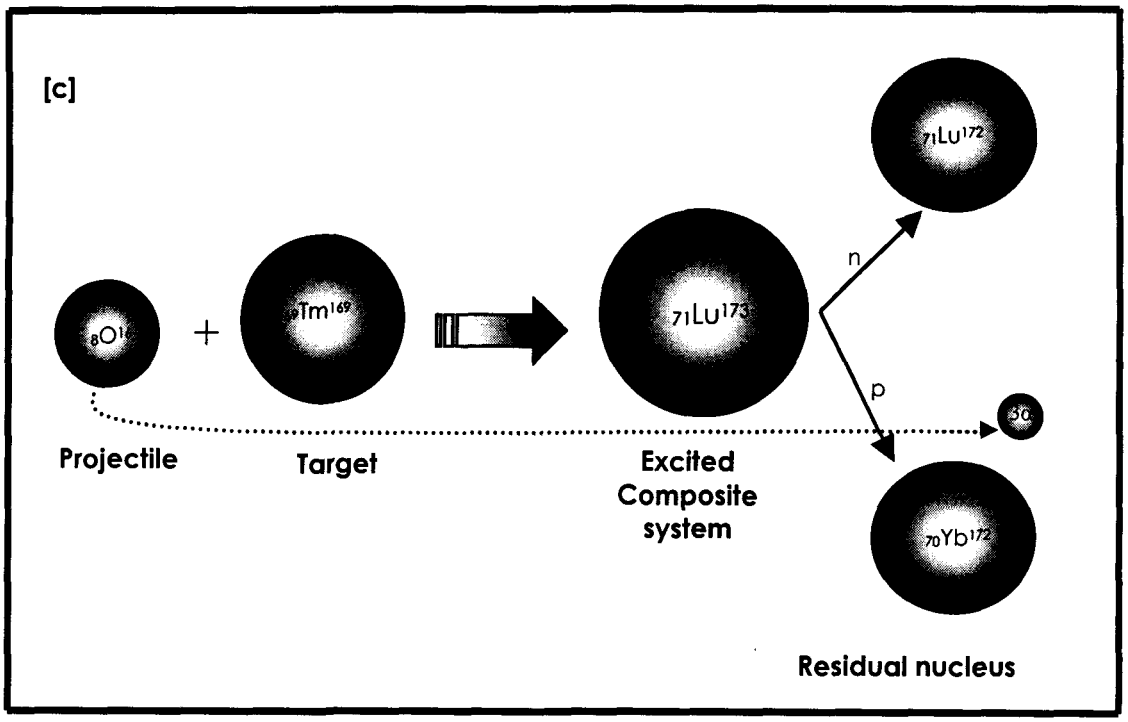

Fig.1.6(b) and (c) Pictorial representation of the fusion of 2α and one α particles respectively with the target.

Recent experiments[16, 17, 18, 19] at energies $\approx$ CB have indicate that Fusion-Fission also plays an important role in HI reactions. The Fusion-Fission is the process of splitting of the composite system which may be formed through various reaction channels like CF or ICF. In fusion-fission reactions the composite system performs oscillations in which its shape changes from spherical to ellipsoidal and back. When a nucleus deforms, the Coulomb energy decreases but at the same time surface energy increases. Therefore, the nucleus tends to assume a spherical shape under the influence of surface tension. However, for an electrically charged drop, such as a nucleus, the Coulomb repulsion is greatest for spherical shape. This repulsion, therefore, tries to deform the nucleus, but at the same time the surface tension tries to keep it spherical. For a heavy nucleus, the repulsion overwhelms the surface tension and consequently the nucleus becomes more distorted. As the sum of Coulomb and surface energy decreases, there are, therefore, no forces that can stop such a nucleus from becoming more and more distorted and finally it may break-up into two or more fragments[14, 15] passing successively through the various stages as shown in Fig.1.7. The time taken in the fissioning process is of the order of the time taken for the nucleus to re-arrange itself in the preparation to dividing into smaller fragments. The fission process may also take place after emitting light nuclear particle/group of particles from the excited composite system.

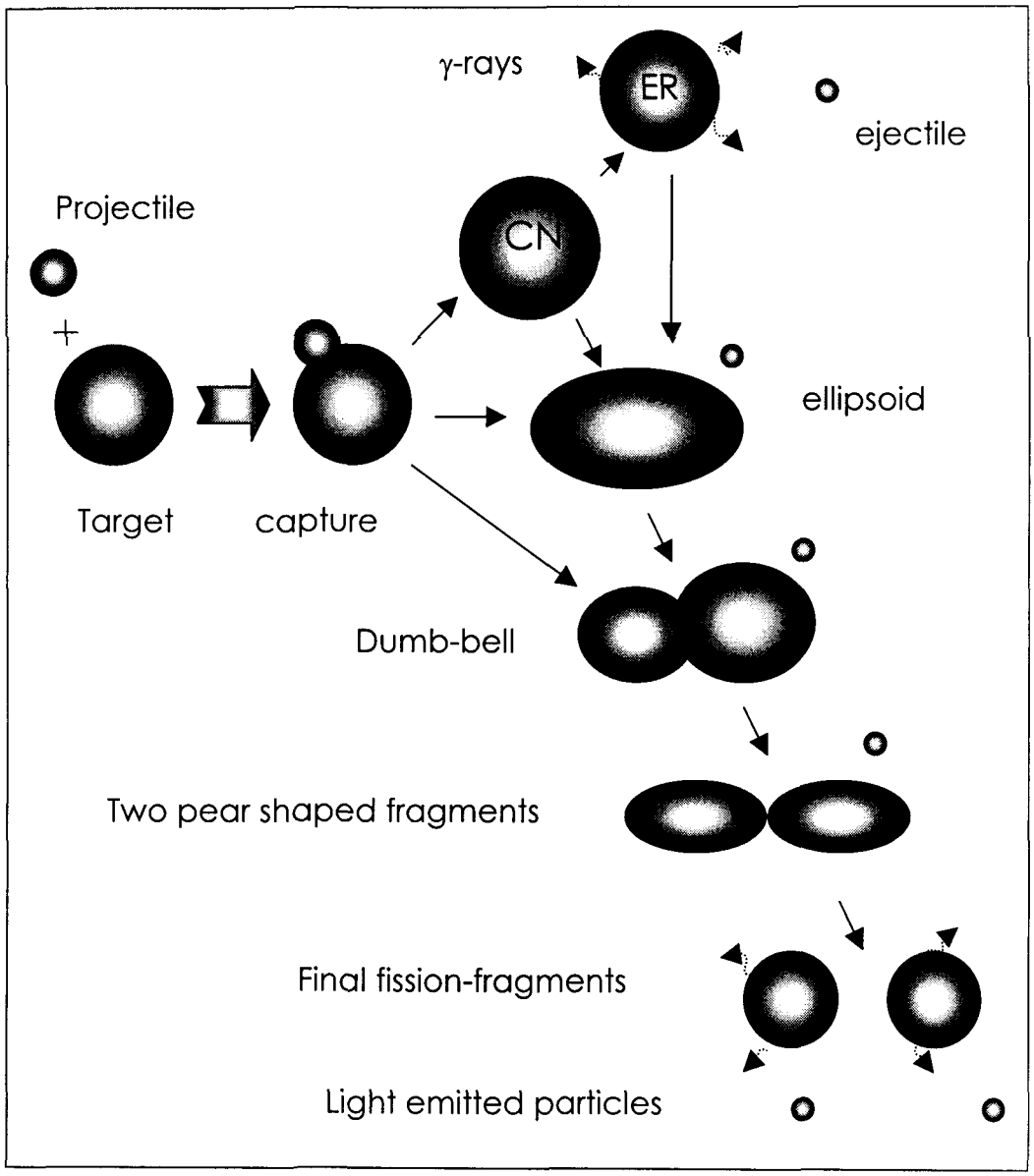

Fig.1.7. Pictorial representation of fusion-fission process passing successively through various stages.

Some recent experimental results[16, 17, 18, 19] have indicated the presence of nuclear fission even at low energies where the fusion is more likely to

be dominant. There are certain aspects that are far from being completely understood, as such the study of fission is still an important and open area of investigation in nuclear physics. Thus, more and more experimental data is required to determine the optimum irradiation conditions for the production yield of various radio-isotopes for better understanging of the phenomena of fission of heavy systems formed in HI reactions. There are two important obserables, e.g., charge and mass distributions which are directly related to collective dynamics of fission. An important aspect of investigation is the stability of fissioning nucleus to mass-asymmetric deformations.

With a view to study the reaction mechanism in HI interactions, a programme of precise measurement of cross-sections[20, 21, 22, 23] for the production of residues due to the complete fusion and incomplete fusion processes has been undertaken by our group. In the present work the cross-sections for the several residues formed through CF and ICF channels in the interaction of $^{16}O+^{169}Tm$ at 7 MeV/nucleon beam energy have been measured in the energy range $\approx$ 70-95 MeV. During the analysis of γ-ray spectra of various samples, it was observed that there are large number of peaks which could not be assigned to the residues populated via CF or ICF processes. As such, in the present work, an attempt has also been made to assign the γ-lines to various residues by analysing the decay curves on the basis of half-lives of residues. Interestingly, a large number of γ-lines were found to be present in the spectra which may be emitted from the residues having masses which are the characteristic of the fission fragments. In the present work the measurement of cros-section for the production of residues expected to be formed

due to fission of the systems formed in the interaction of $^{16}O+^{169}Tm$ at ≈ 95 MeV are also reported. The cross-section data of such products are important for the production of specific radio-active ion beams and are required in the upgrading of accelerators. These cross-sections are also in demand for the development of accelerator driven subcritical reactors popularly known as energy amplifiers[24].

The experiment has been performed at the Nuclear Science Centre (NSC), New Delhi, India. The details of experiment and technique employed are given in the $2nd$ chapter of this dissertation. The experimental mesurements are described in $3rd$ chapter. The $4th$ chapter of this dissertation deals with the results and conlusions of the present mesurements. References are given at the end of each chapter.

References

[1] J. J. Thomson, Phil. Mag., 44 (1897) 293.

[2] E. Rutherford, Phil. Mag., 21 (1911) 669.

[3] H. Becquerel, Comp. Rend., 122 (1896) 450.

[4] E. Rutherford, Phil. Mag., 37 (1919) 581.

[5] E. Rutherford, Phil. Mag., 37 (1919) 537.

[6] N. Bohr, Nature, 137 (1936) 344.

[7] S. N. Ghoshal, Phy. Rev. 80 (1950) 939.

[8] M. Blann, Phys. Lett. 27 (1971) 337.

[9] H. D. Bhardwaj, Ph.D. Thesis (1985), AMU, Aligarh, India.

[10] B. P. Singh, Ph.D. Thesis (1991), AMU, Aligarh, India.

[11] P. E. Hodgson, E. Gadioli and E. Gadioli Erba, Introductory Nuclear Physics, Chapter 23, Clarendon Press , Oxford (1997).

[12] H. C. Britt and A. R. Quinton, Phys. Rev. 124 (1961) 877.

[13] J. Wilczynski et. al., Nucl. Phys. A373 (1982) 109.

[14] L. Meitner and O. R. Frisch, Nature 143 (1939) 239.

[15] N. Bohr and J. Wheeler, Phys. Rev. 56 (1939) 426.

[16] D. J. Hinde et. al., Phys. Rev. C 39 (1989) 2268.

[17] D. J. Hinde et. al., Phys. Rev. C 45 (1992) 1229.

[18] L. M. Pant et. al., Eur. Phys. J. A 11 (2001) 47.

[19] R. Tripathi et. al., Phys. Rev. C 69 (2004) 024613.

[20] Sunita Gupta et. al., Phys. Rev. C 61 (2000) 064613.

[21] Sunita Gupta et. al., Int. J. of Modern Phys. E 10, No. 6 (2001) 1-9.

[22] Manoj Kumar Sharma et. al., J. Phys. Soc. of Japan, 72 (2003) 1917.

[23] Manoj Kumar Sharma et. al., Phys. Rev. C 70 (2004) 044606.

[24] C. Rubbia et. al., Conceptual Design of a Fast Neutron Operated High Power Energy Amplifier, Report CERN/AT/95-94 (ET) 1995.

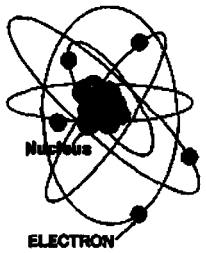

②Experimental details

Excitation functions for several reactions in $^{16}O+^{169}Tm$ have been measured in the energy range $\approx$ 70-95 MeV. Further in the present work, reaction cross-sections for the production of a large number of fragments produced in the fission of composite systems formed via CF & ICF of $^{16}O+^{169}Tm$ system at $\approx$ 95MeV beam energy have also been measured using activation technique[1]. The experiment has been performed at $15-UDPelletron$ *Accelerator* facility of Nuclear Science Center(NSC), New Delhi. Brief details of pelletron accelerator, activation technique, sample preperation, irradiation etc., are given in the following section.

2.1 Pelletron Accelerator

A schematic diagram of $15-UD$ *Pelletron Accelerator* at NSC, New Delhi is shown in the Fig.2.1.1. It is based on the working principle of Van de-Graff electrostatic accelerator, capable to accelerate the charged particles or ions from hydrogen to uranium except the inert gases in the energy range from few tens of MeV to few hundred MeV depending on the type of ion species. The pelletron accelerator is installed in a vertical fashion in a stainless steel tank, at high pressure ($\approx$10 atm). The tank is $\approx$ 26.5 m high and 5.5 m in diameter. There is a high voltage terminal in the middle of the tank whose potential can hold from 4 to 16MV.

The high voltage terminal housed in the high pressure tank which is filled with SF_6 gas of high dielectric constant, to prevent the break down of high voltage. The uniform potential gradient required for accelerating ions is maintained by equipotential rings through the accelerating tube. The

singly charged negative ions from the $MC - SNICS$ (multi cathod-source of negative ions by cesium sputtering) ion source are injected by the injector magnet into the accelerator tube. This injector magnet not only injects the beam into the accelerator but it serves to select required ion beam and focuses the beam in both axial and radial planes (commonly known as double focussing). The focused and anlysed negative ion beam is attracted by the positive terminal. Due to the attraction, the negative ion beam gets accelerated from the ground potential to the terminal of high positive potential. The ions coming from the negative ion source get acceleration and acquire additional energy V_t up-to high voltage terminal. The beam is then made to pass through a charge stripper (gas or foil) which is accommodated inside the high voltage terminal, where the beam looses some electrons and, therefore, the ions become positively charged. Since the high voltage terminal is at positive potential so the positive ions are repelled and are then accelerated below the terminal towards the ground potential.

If the charge state of the positive ions after passing through the high voltage (V_t) terminal is q, then the energy gain in the acceleration below the terminal to the ground potential is qV_t. Therefore, after passing through the two stages of acceleration, the final energy of the ion beam is given by,

$$E = E_0 + (q + 1)V_t \tag{5}$$

where, E_0 is the energy of ions before acceleration, q is the charge state of the ions after stripping and V_t is the terminal potential. Since, in most of the cases E_0 is much smaller than the final energy of the beam, therefore, it may be neglected.

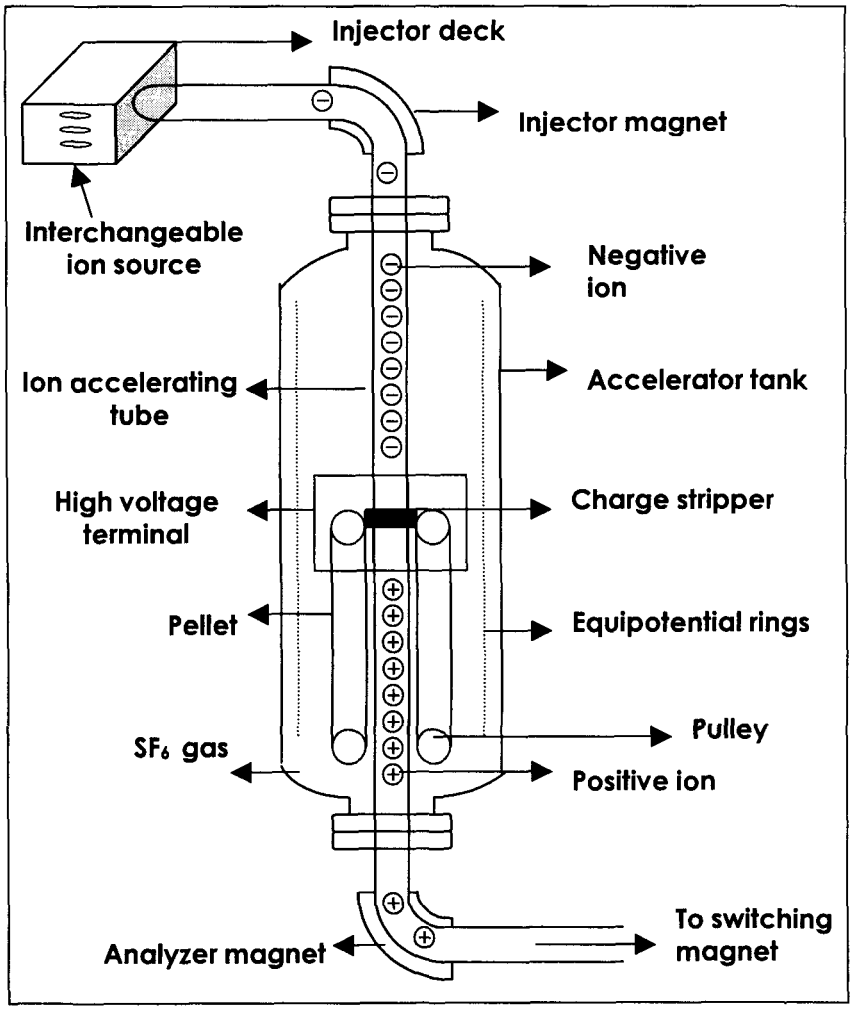

Fig.2.1.1 A schematic diagram of Pelletron accelerator at NSC.

The accelerated ion beam is then passed to the analysing magnet and the slit. This arrangement makes the beam clean by providing an energy selection so that one can get particular ion beam of desired energy. The ion beam may then be directed towards the desired experimental area by the switching magnet. This magnet is the horizontal bending semicircular magnet which bends the beam into the various beam lines at different angles. A schematic block diagram of different beam lines of 15UD-Pelletron accelerator facility at NSC is shown in the Fig.2.1.2.

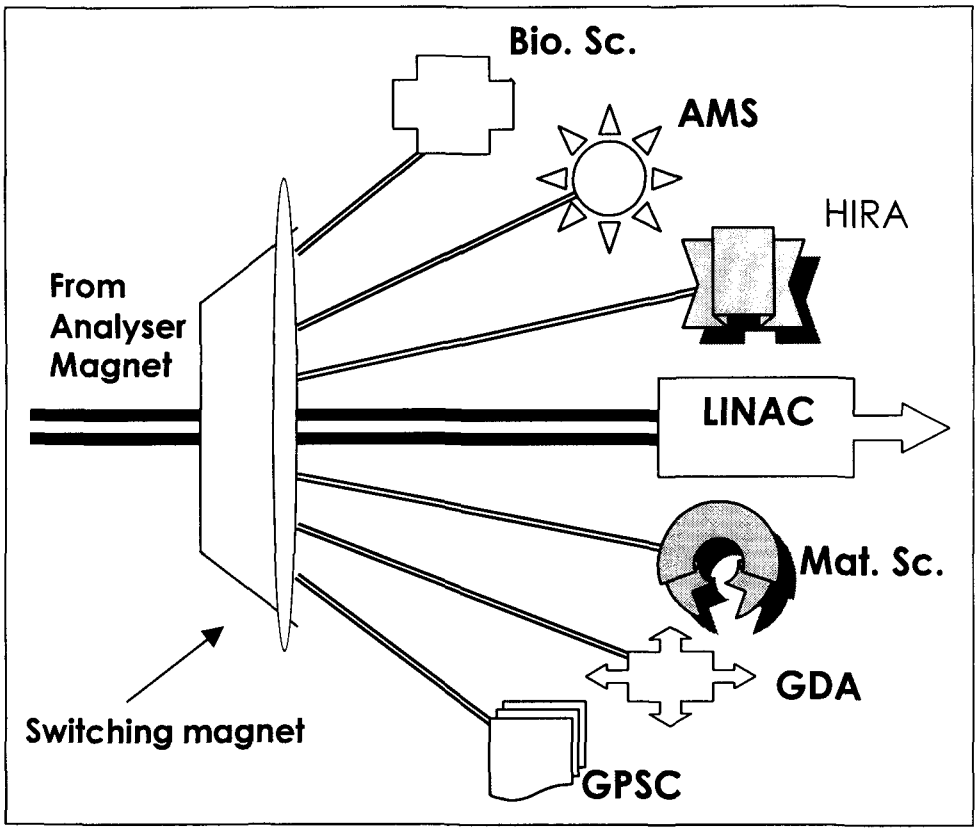

Fig.2.1.2 A schematic diagram of different beam lines at NSC Pelletron facility.

2.2 Activation technique

During the last few decades, activation analysis[1] has been establised as a powerful and sensitive tool for measuring the concentration of constituents in a given sample by measuring the charateristic radiations emitted by the radio-active nuclides. The unique nuclear properties of each activation product provides a specific way for its identification and measurement. Activation technique is based on the formation of radio-active nuclides as a result of interaction between two nuclear particles. In this technique a sample may

be irradiated in a fixed geometry by placing the target material normal to the incident beam. After irradiation, several activities may be produced in the samples due to the different reactions taking place as a consequence of energetic beam interaction. The mesurement of the cross-sections of the produced residues may be performed by following the activities induced in the samples after irradiation. The main feature of this technique is that, the cross-sections for more than one reaction may be measured in a single irradiation thus reducing the beam time requirements. However, this technique is limited only for the reaction products having measurable half lives. The activation technique has many applications[2] in various fields of nuclear research and applied sciences due to its selectivity, sensitivity and simplicity.

The recent growth of activation analysis is mainly due to the advancement in detection techniques and nuclear electronics. Although, the activation analysis is quite simple and accurate but some times it becomes complicated due to the presence of radiations of slightly different energies from more than one reaction products. The contribution of different isotopes may, however, be seperated on the basis of half-lives by following the activities for a considerably longer period and then analysing the decay curves. The activation analysis requires the precise knowledge of energy levels and the decay schemes of the residual nuclei. The proper choice of the target material, projectile type, energy of the projectile, time of irradiation and half life of the induced activities are of considerable importance.

2.3 Sample preparation

The target of natural ^{169}Tm were prepared by employing vacuum evaporation technique. This technique is commonly used for the thin film target preparation. In the above technique, the material to be deposited is heated to a high temperature, in an evacuted chamber, and is condensed on a suitable substrate. An electron gun is generally used for heating. The thicknesses of ^{169}Tm samples were $\approx 0.6 mg/cm^2$. These samples were deposited on Al-foils of thickness ($\approx 1.5 mg/cm^2$). The thickness of the samples were measured by employing α-transmission method, which is based on the measurement of energy loss of α-particles while passing through the sample. The α-particles of energy 5.485 MeV from ^{241}Am source were used for these measurements. During irradiation by HI beam the Al-backing served as catcher foil, so that the recoiling residues produced due to nuclear reactions including complete fusion, incomplete fusion and fission may be trapped in the catcher thickness. The samples were cut in to the size of $1.2 \text{x} 1.2 cm^2$ and were pasted on Al-holders having concentric hole of 1.0 cm diameter. The Al-holders were used for rapid dissipation of heat produced during irradiation.

2.4 Irradiation

The irradiation has been performed in the General Purpose Scattering Chamber($GPSC$) of 1.5m diameter having in vacuume transfer facility at the NSC, New Delhi. The advantage of in-vacuum transfer facility is that the delay time between the stop of irradiation and the begining of counting may be minimised. A stack of five samples with target material facing the

beam was placed normal to the beam direction so that the recoiling nuclei may be trapped in the thickness of Al-catcher foil. In the present work, a stack of samples of ^{169}Tm was irradiated by $\approx$ 95MeV oxygen (^{16}O) beam of +7 charge state. Keeping in view the half-lives of interest, the irradiation was carried out for $\approx$8hrs duration with a beam current $\approx$30nA. The total charge collected in the Faraday cup has been used to calculate the flux of beam. A typical arrangement of target catcher assembly used for irradiation in the present experiment is shown in Fig.2.4.1.

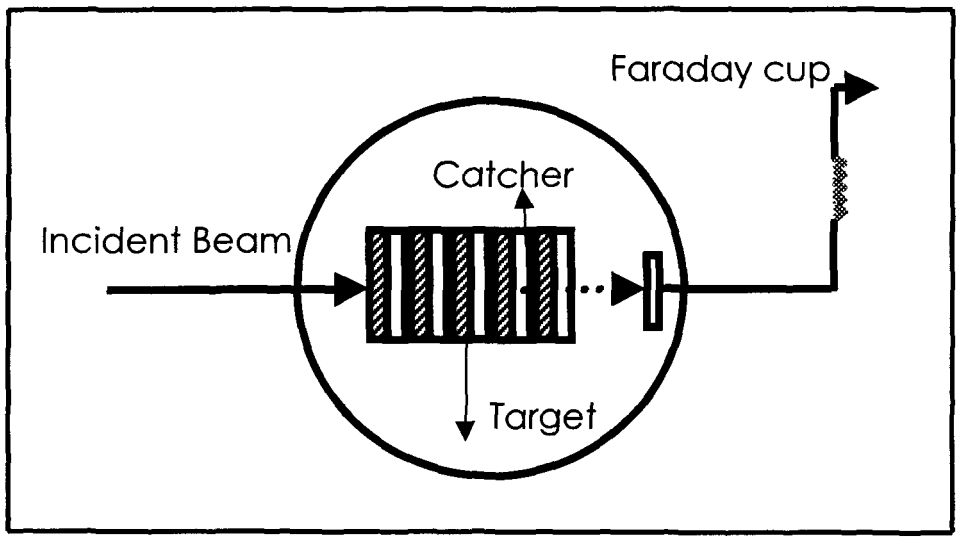

Fig.2.4.1 Typical arrangement for irradiation of stack.

2.5 Calibration and efficiency determination of γ-ray spectrometer

A detector of high resolution and proper calibration is the essential tool to identify the characteristic γ-rays of radio-active residues. In the present

experiment, the induced activities in the irradiated samples were analysed by using High Purity Germanium (HPGe) Detector of 100c.c. active volume coupled to a PC through CAMAC based FREEDOM software[3]. The resolution of the detector was ≈2keV for 1.33MeV γ-ray of ^{60}Co source. A typical block diagram of γ-ray spectrometer set-up used is given in Fig.2.5.1.

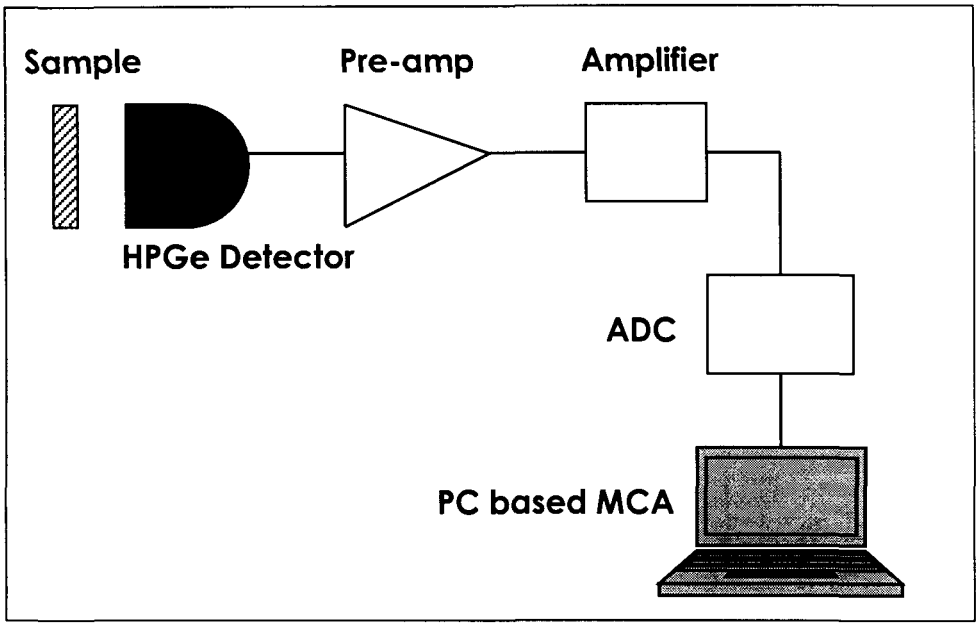

Fig.2.5.1 A typical block diagram of γ-ray spectrometer setup used for the calibration and γ-ray spectrometry.

The detector was pre-calibrated by using standard γ-ray sources(i.e., ^{22}Na, ^{54}Mn, ^{57}Co, ^{60}Co, ^{133}Ba, ^{137}Cs and ^{152}Eu) of known strengths. The geometry dependent efficiency(G_ε) of HPGe detector at a given energy was

calculated by using the expression,

$$G_\varepsilon = \frac{N_0}{N_{a0}\theta e^{(-\lambda t)}} \tag{6}$$

Where, N_0 is the observed disintegration rate of the standard γ-ray source at the time of measurement, N_{a0} is the disintegration rate at the time of manufacture, λ is the deacy constant, t is the lapse time between the manufacture of the source and the start of the counting and θ is the braching ratio of the characteristic γ-rays.

The prominent γ-rays[4] of ^{22}Na, ^{54}Mn, ^{57}Co, ^{60}Co, ^{133}Ba, ^{137}Cs and ^{152}Eu sources used for the calibration and efficiency determination in the present measurements are given in Table-2.5.1

Table 2.5.1 The energies and absolute intensities of prominent γ-rays from standard sources

S.No.	Source	γ-ray energy (keV)	Absolute Intensity (%)
1.	^{22}Na	1274.53	99.93
2.	^{54}Mn	834.82	99.97
3.	^{57}Co	122.06	85.50
		136.47	10.69
4.	^{60}Co	1173.23	99.90
		1332.50	99.98

S.No.	Source	γ-ray energy (keV)	Absolute Intensity (%)
5.	^{133}Ba	308.24	10.10
		423.40	8.20
		632.42	9.00
		691.08	6.50
6.	^{137}Cs	661.66	85.21
7.	^{152}Eu	121.78	28.40
		244.69	7.51
		344.29	26.60
		443.89	2.80
		778.92	12.98
		964.11	14.50
		1112.08	13.60
		1299.16	1.63
		1408.00	20.80

In the present work, the standard γ-sources and irradiated sample foils were counted in the same geometry. The distance between source and detector for different irradiated samples were kept different depending on the intensity of the induced activity. Care was taken to keep the dead time of the detector less than 10% by suitably adjusting the source-detector separation. The geometry dependent efficiency curves for the γ-rays of different energies at 2cm and 3cm source-detector separations are plotted by using the ORIGIN graphics software and are shown in Fig.2.5.2.

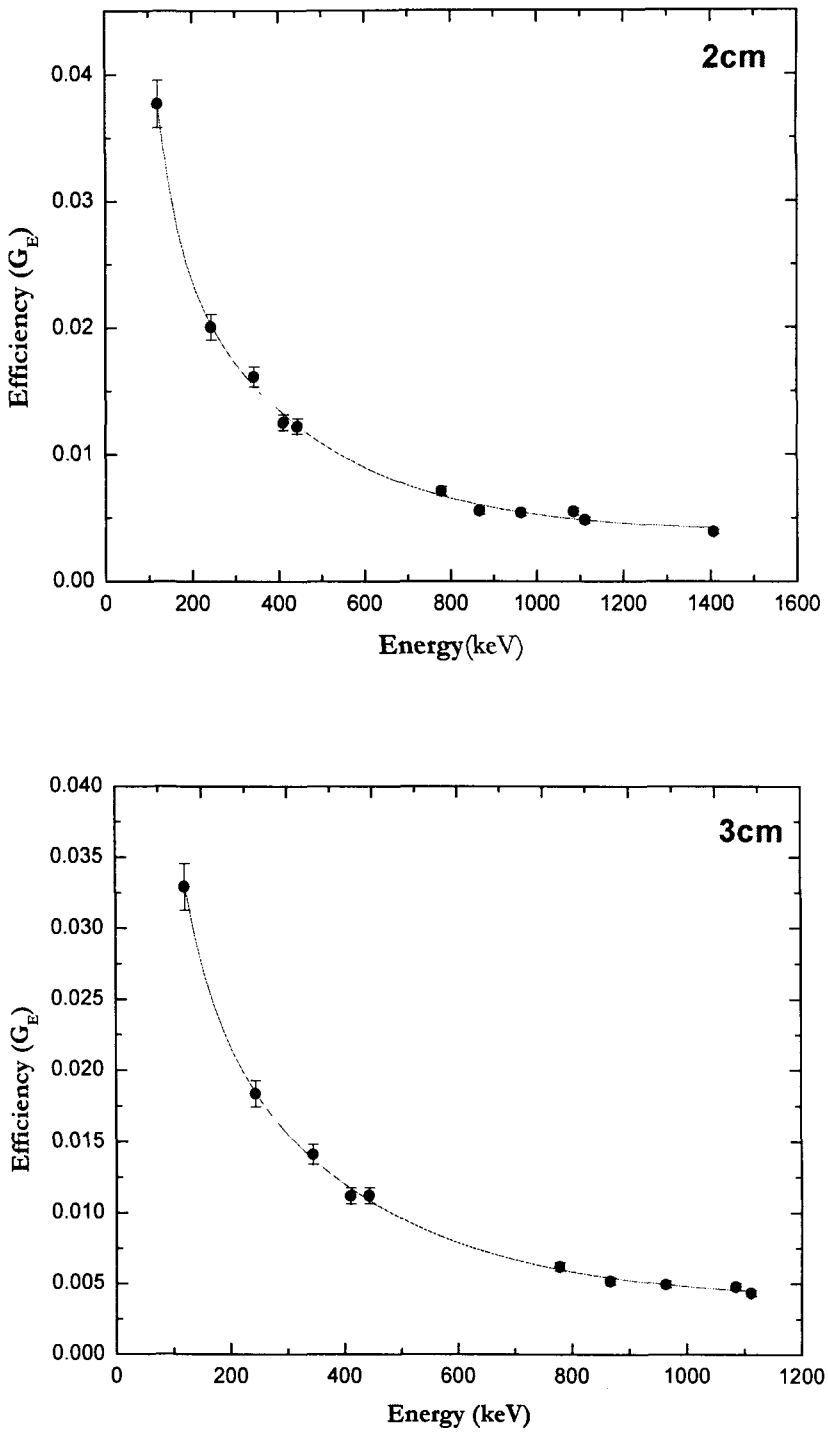

Fig.2.5.2 Typical geometry dependent efficiency curves for 2 cm and 3 cm source-detector distance as a function of γ-ray energy.

The experimental geometry dependent efficiency data is found to be best fitted with a polynomial of degree 5, having the following form,

$$G_\epsilon = a_0 + a_1X + a_2X^2 + a_3X^3 + a_4X^4 + a_5X^5 \quad (7)$$

where; a_0, a_1, a_2, a_3, a_4 and a_5 are the coefficients having different values for different source-detector distance and X is the characteristic γ-ray energy.

2.6 Experimental uncertainties

Errors are the part of every experiment. Some of the factors likely to introduce errors in the present measurements are given here.

1. Non-uniform thickness of the target material and an inaccurate estimate of foil thikness may lead to the uncertainty in the determination of the number of target nuclei. To check the uniformity of the sample, thickness of the samples was measured at different positions by α-transmission method. It is estimated from this analysis that the error in the thickness of the sample material is expected to be less than 1%.

2. Fluctuations in the beam current may result in the variation of incident flux. Proper care was taken to keep beam current constant and any accidental stop of beam or appreciable fluctuation of the beam intensity was recorded and taken care of, at the time of calculating the total time of irradiation and average beam current.

3. In determining the count rate, the dead time may introduce some errors. In the presnt work, dead time was kept less than 10% by suitably adjusting sample-detector distance.

4. Uncertainty in the fitting of the efficiency curve (less than 3%) and solid angle effect (less than 2%) may lead to inaccuracy in the measurement of detector efficiency[5]. The measured efficiency may be inaccurate on account of the statistical errors of counting of the standard source. These were minimised by accumulating the data for a longer time ($\approx$3000 sec). The error in efficiency determination due to the statistical fluctuations in counts is estimated to be less than 2%.

5. Error in the incident beam energy has been determined by calculating the energy spread in half thickness of the sample with the help of Stopping Power Tables of Northcliffe and Schilling[6].

6. The losses of product nuclei recoiling out of the target may introduce large errors in the measured cross-sections. The thickness of the catcher foil was sufficient to stop even the most energetic residue, however, in the present measurements both the sample and the catcher foil were counted together and hence the loss due to the recoiling of nuclei is avoided.

These errors exclude the uncertainty of the nuclear data like branching ratio, deacay constant etc., which have been taken from the Table of Isotopes[4].

References

[1] R. C. Kotch, Activation Analysis Handbook, Academic Press, New York and London, 1960.

[2] E. V. Sayre, Ann. Rev. Nucl. Sci. 13 (1963) 145.

[3] FREEDOM: Data Acquisition and Analysis System designed to support the accelerator based experiments at the Nuclear Science Centre, New Delhi, India.

[4] E. Brown and R. B. Firestone, Table of Isotopes, Wiley, New York, 1986.

[5] R. P. Gardner et. al., Nucl. Instrum. Method 93 (1971) 163.

[6] L. C. Northcliffe and R. F. Schilling, Atomic Data Nuclear Data Table A7 (1970) 264.

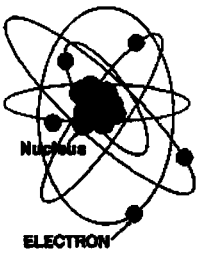

③Measurements

A nuclear reaction is initiated when an energetic projectile interacts with a target nucleus. A change in the composition and or energy of the target nucleus takes place, as a result different reaction products may be produced. Reaction cross-section is a measure of the probability of occurrence of a particular nuclear reaction. Experimentally, the nuclear reaction cross-section may be defined as the number of events of a given type $X(a,b)Y$ per unit area per unit target nucleus per unit time and is usually denoted by σ. The cross-section is expressed in units of barn which is equal to $10^{-24}cm^2$. Mathematically, the reaction cross-section may be represented as[1],

$$\sigma_r = \frac{Number\ of\ events\ of\ a\ given\ type\ X(a,b)Y/area}{N_0\ \phi\ t} \tag{8}$$

Where, N_0 is the number of nuclei in the target, ϕ is the flux of incident beam and t is the time of bombardment. In order to determine the cross-section of a particular reaction, the quantities given in the denominator of the above equation are known and the quantities in the numerator i.e., the number of events of a given type $X(a,b)Y$ are required to be measured. The number of events of a given type may be obtained from (a)On-line measurements, by recording the outgoing particles directly using particle telescopes accomodated in the irradiation chamber or (b)Off-line measurements, by following the activities induced in the irradiated samples, in case the radioactive residues are of measurable half-lives. The on-line measurements are quite complicated due to the large background in general. In the present work off-line γ-spectroscopy has been used for the measurement of reaction cross-sections.

3.1 Formulation

Irradiation of a sample by a particle beam may initiate various reactions in it and many isotopes are formed by the process of transmutation. The rate of formation (N) of a particular activation product may be given by the following expression,

$$N = N_0 \phi \sigma_r \tag{9}$$

where; ϕ is the flux of incident beam, N_0 is the initial number of nuclei in the target/sample and σ_r is the reaction cross-section for that particular channel.

The disintegration rate of the induced activity in a sample after a time t from the stop of irradiation may be given as,

$$\left[\frac{dN}{dt}\right]_t = N\frac{[1 - exp(-\lambda t_1)]}{exp(\lambda t)} \tag{10}$$

where; t_1 is the time of irradiation and λ is the decay constant of the induced activity given as,

$$\lambda = \frac{ln2}{t_{1/2}} \tag{11}$$

The factor $[1 - exp(-\lambda t_1)]$ is called the saturation correction. It should also be considerd that some radionuclei produce may also decay during the irradiation time, therefore, the number of decays of the induced activity in a very small time dt may be given as,

$$dN = N\frac{[1 - exp(-\lambda t_1)]}{exp(\lambda t)}dt \tag{12}$$

If activity induced in the irradiated sample is recorded for time duration t_3 after a lapse time t_2, then the number of nuclei decayed in time between t_2

to (t_2+t_3) may be given as,

$$C = N\frac{[1 - exp(-\lambda t_1)][1 - exp(-\lambda t_3)]}{\lambda exp(\lambda t_2)} \tag{13}$$

If the activity induced in the sample is recorded by a γ-ray spectrometer of efficiency G_ε, then, absolute count rate C and observed counting rate may be related as,

$$C = \frac{A}{G_\varepsilon \theta K} \tag{14}$$

Where, θ is the branching ratio of the characteristic γ-ray and K=$[1 - exp(-\mu d)]/\mu d$ is the self absorption correction factor for the material of the sample of thickness d (gm/cm^2) and of absorption coefficient μ (cm^2/gm). Thus, σ_r can be written as[2],

$$\sigma_r = \frac{A\lambda exp(\lambda t_2)}{N_0 \theta \phi G_E K[1 - exp(-\lambda t_1)][1 - exp(-\lambda t_3)]} \tag{15}$$

Also, the count rate at the time of stop of irradiation $C_{t=0}$ can be given as,

$$C_{t=0} = \frac{A\lambda exp(\lambda t_2)}{[1 - exp(-\lambda t_3)]} \tag{16}$$

The reaction cross-section σ_r may be written with the help of above equations as[3],

$$\sigma_r = \frac{C_{t=0}}{N_0 \theta \phi G_E K[1 - exp(-\lambda t_1)]} \tag{17}$$

A FORTRAN program EXP-SIGMA based on the above formulation has been used for the determination of the reaction cross-sections of the populated reaction channels.

3.2 Identification of reaction residues

In HI reaction, residue may be formed due to CF and ICF processes. These residues may also under go fission. Hence the ultimate residues are likely to decay to the ground state by emitting characteristic γ-rays. In order to determine the production cross-section of these residues, first of all it is desirable to identify them. As discussed earlier the residual nuclei may be identified by their characteristic γ-rays after the irradiation of the sample is over. This is a very specific way for the identification of reaction residues because each radio-active isotope has a unique decay mode. Thus, the observed intensity of induced activity is a measure of the production cross-section of that particular reaction residue. In order to identify various residues the preliminary analysis was performed by identifying the γ-rays of the residues. However, since there were several residues which may emit γ-ray of nearly same energies, thus simple energy identification may not be enough.

As a typical example the γ-ray spectrum of $^{16}O+^{169}Tm$ bombarded at $\approx$ 95 MeV is shown in Figs.3.2.1(a) & (b). As can be seen from these figures different peaks in the spectrum may be assigned to residues produced via different channels. The γ-rays spectra of the irradiated samples were recorded at increasing times. The intensity of the photo-peaks were plotted as a function of time to get the half-lives of the residues. Thus, in the present work the residues were identified not only by their characteristic γ-rays but also by their measured half-lives.

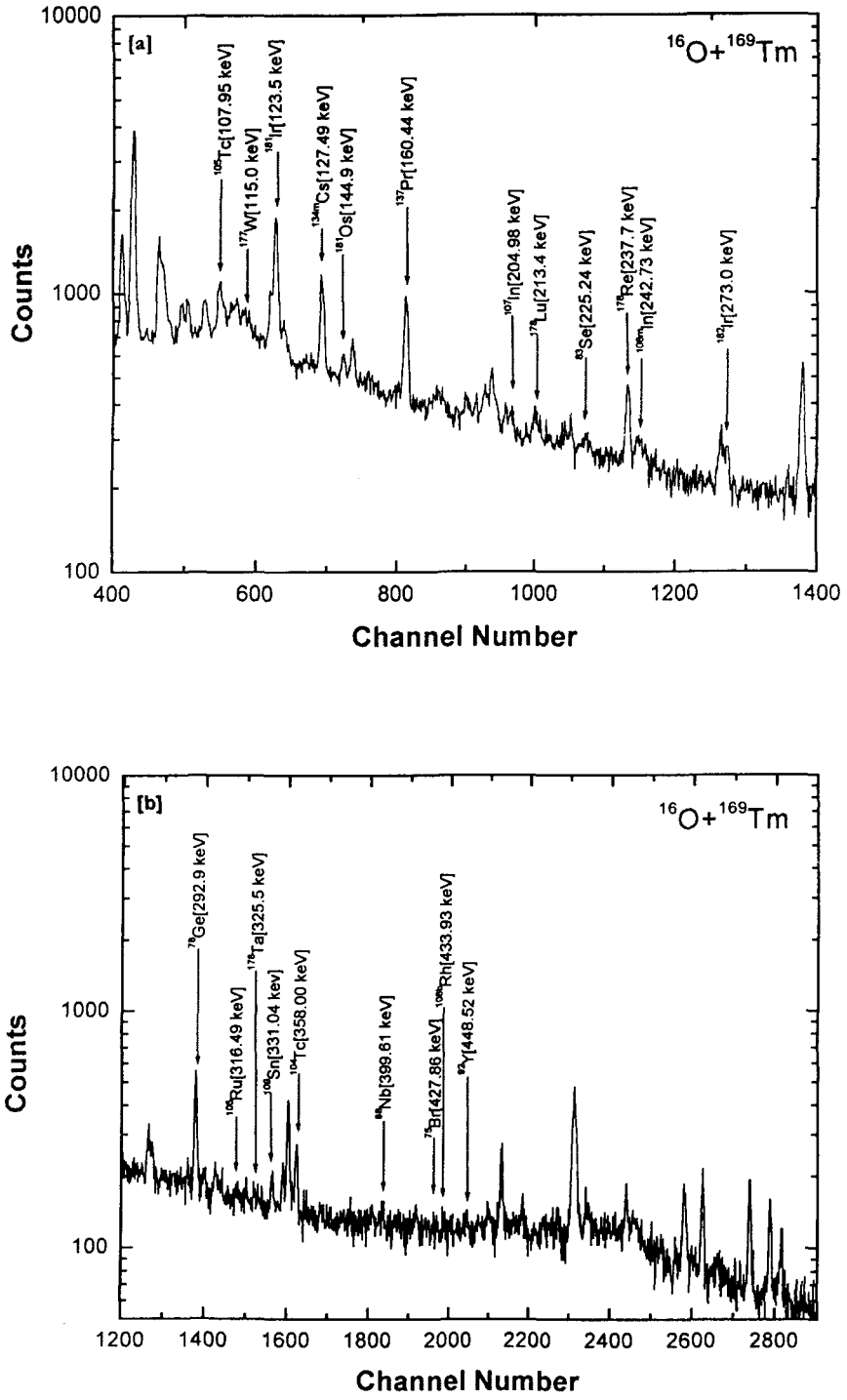

Fig.3.2.1(a). Typical γ-ray spectrum of $^{16}O+^{169}Tm$ bombarded at $\approx$ 95 MeV beam energy.

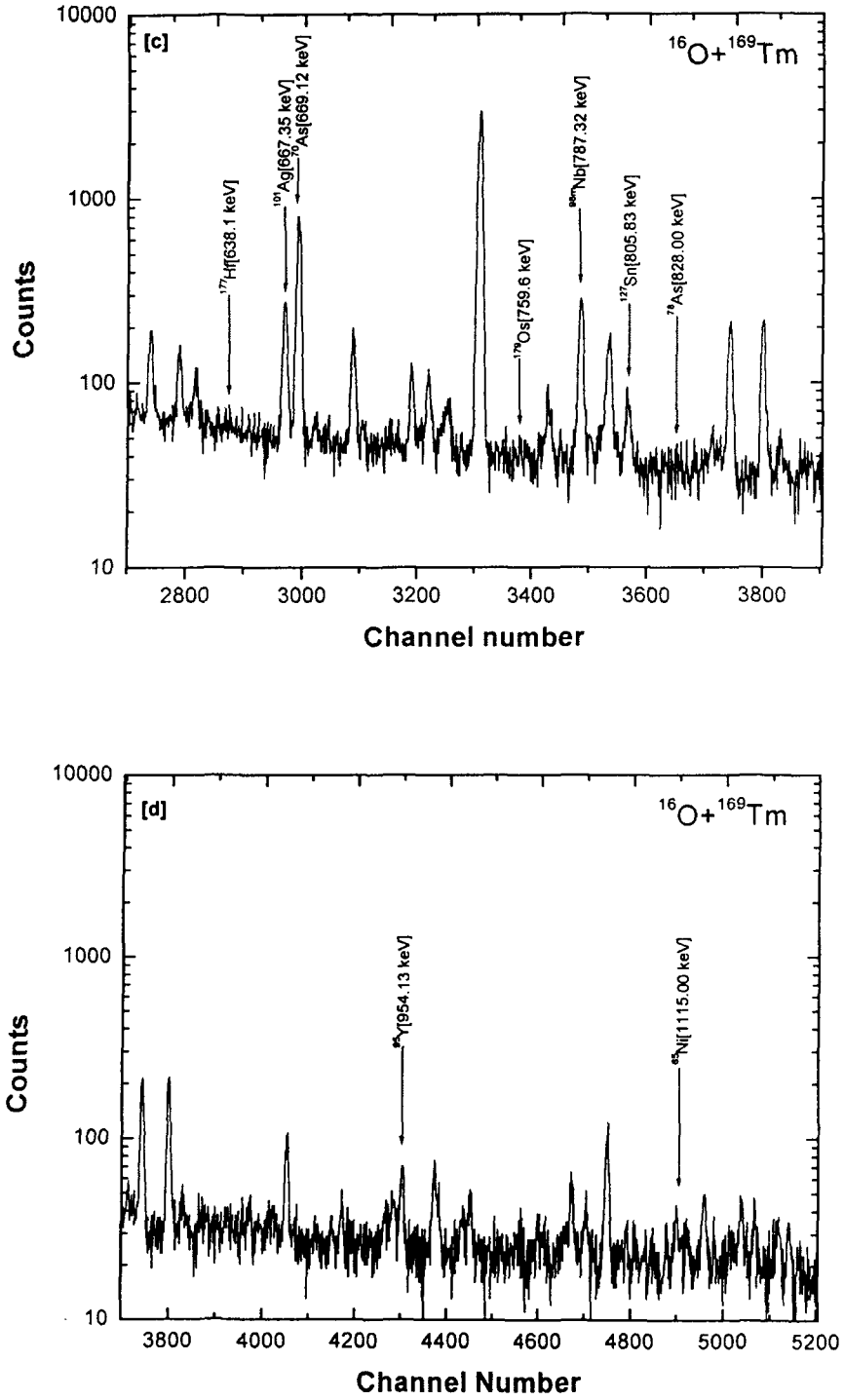

Fig.3.2.1(b). Typical γ-ray spectrum of $^{16}O+^{169}Tm$ bombarded at $\approx$ 95 MeV beam energy.

In the cases, where the residues emit γ-rays of nearly same energy but have different half-lives, residues were identified on the basis of half-lives obtained from the analysis of the deacy curves of composite activity. As a typical example the observed decay curves of several residues are given in Figs.3.2.2 to 3.2.5. The contribution of each isotope in the composite activity was separated by using the deacy curves and following the activities for a long period. The nuclear data of radio-nuclides which have been used in the analysis are taken from the Table of Isotopes[4] and Nuclear Wallet Card[5].

3.3 Assignment of reaction channels to residues

In the present work an attempt has been made to analyse the γ-ray spectrum and assign the peaks to different reaction channels. Lists of identified residues, reaction channels, half-lives of residues, their γ-ray energies and branching ratios are given in Tables-3.3.1 to 3.3.3.

Table 3.3.1 Residues which are expected to be formed via complete fusion(CF)

Residue	Reaction	half-life	γ-ray energy(keV)	branching ratio(%)
^{181}Ir	$^{169}Tm(O,4n)$	5 m	123.5	28
^{182}Ir	$^{169}Tm(O,3n)$	15 m	273.0	43
^{181}Os	$^{169}Tm(O,p3n)$	105 m	144.9	1.4
^{179}Os	$^{169}Tm(O,p5n)$	6.5 m	759.6	68
^{178}Lu	$^{169}Tm(O,6pn)$	23.1 m	213.4	81.3

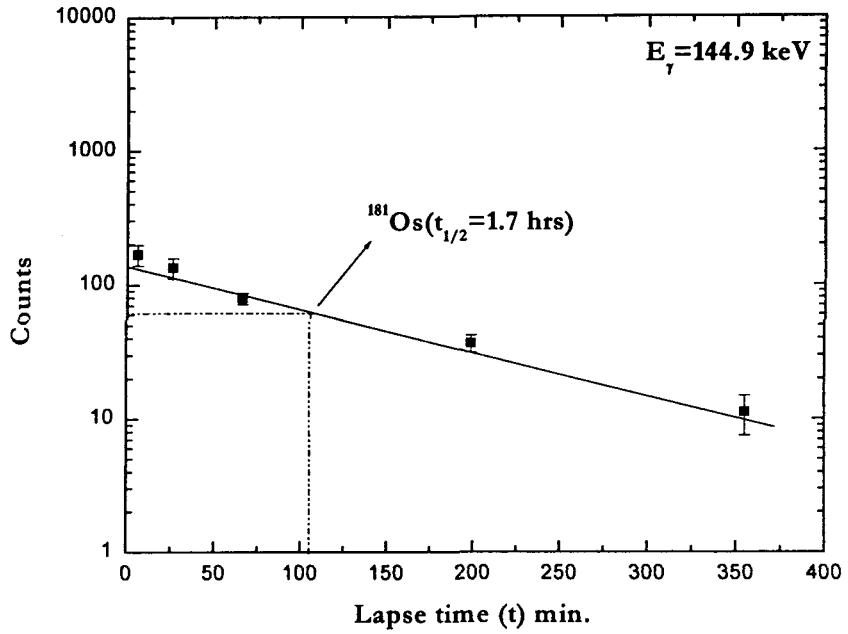

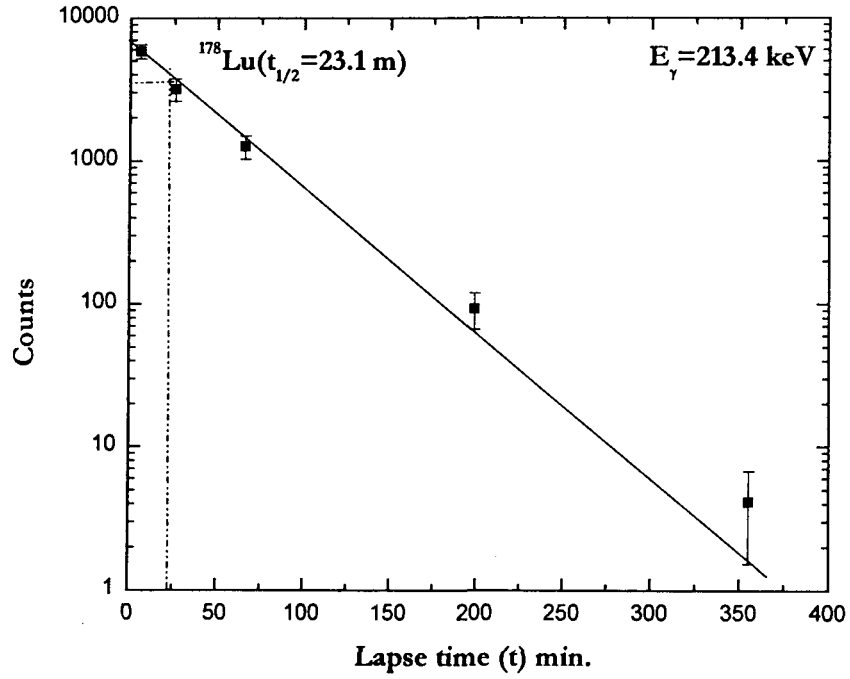

Fig.3.2.2 Typical decay curves of several residues. .

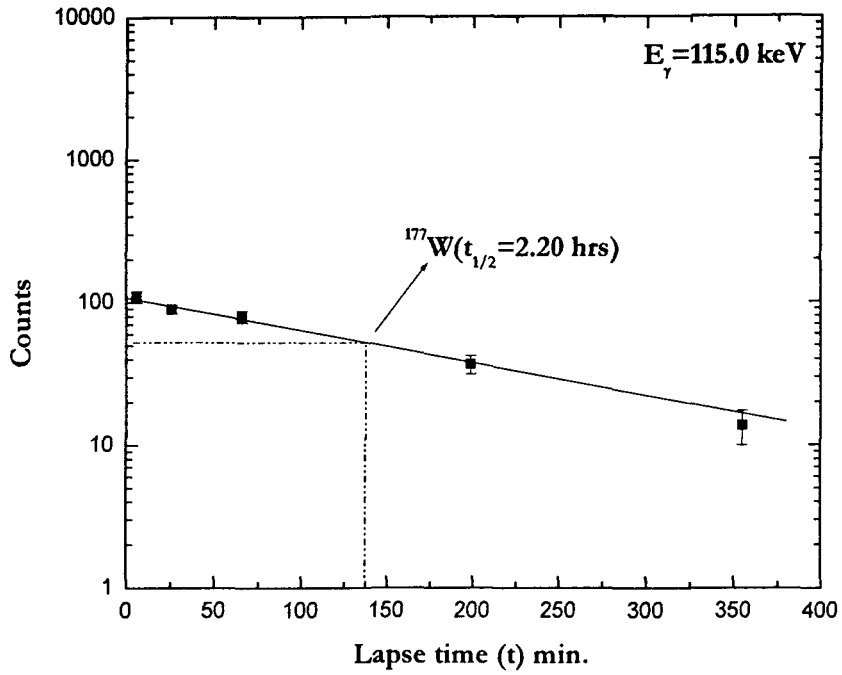

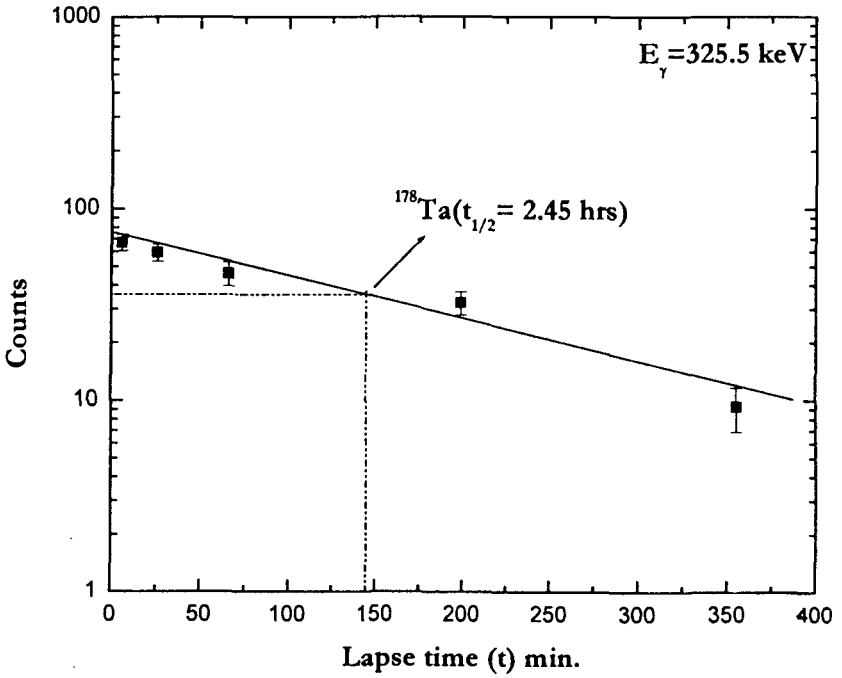

Fig.3.2.3 Typical decay curves of several residues. .

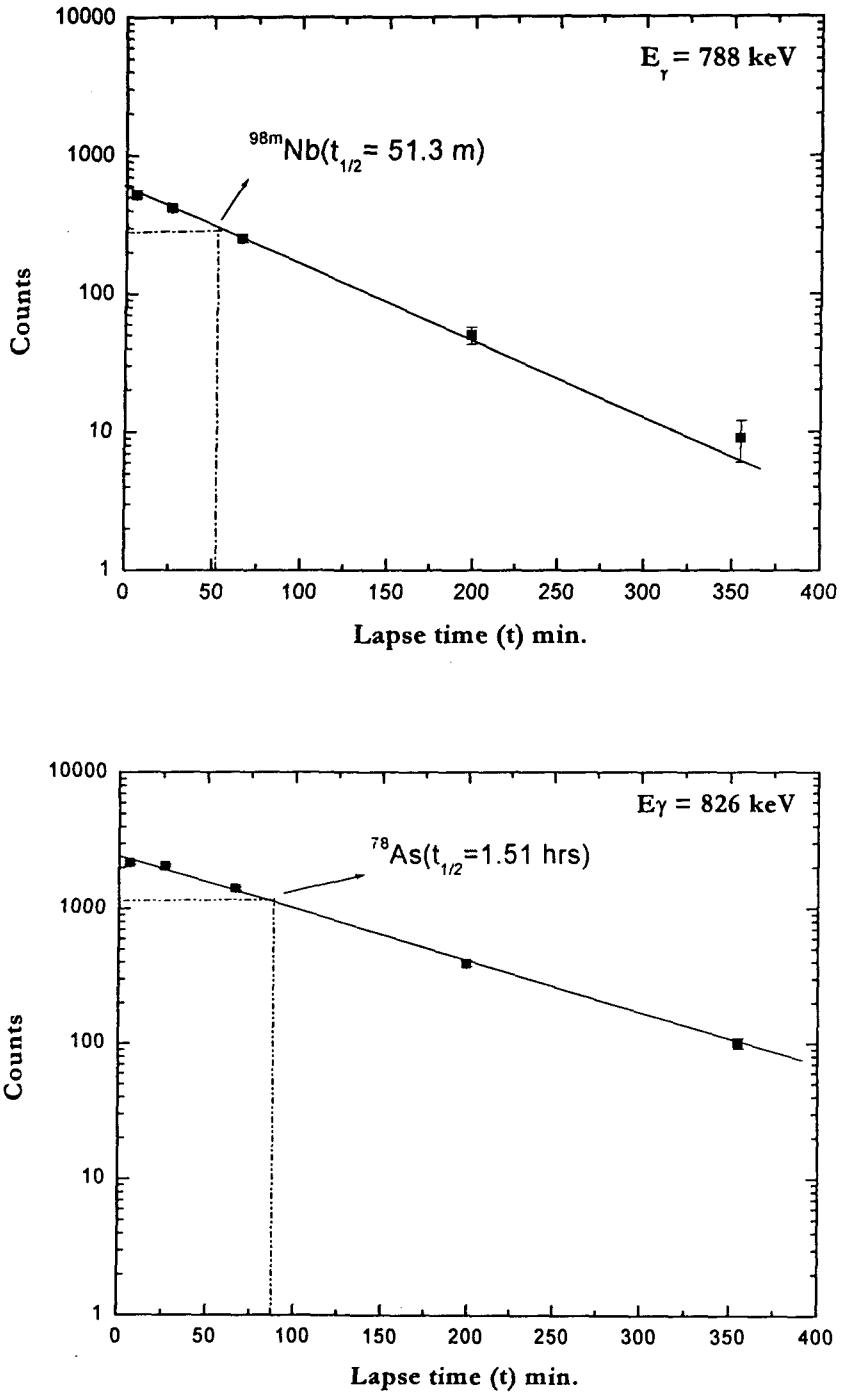

Fig.3.2.4 Typical decay curves of several residues.

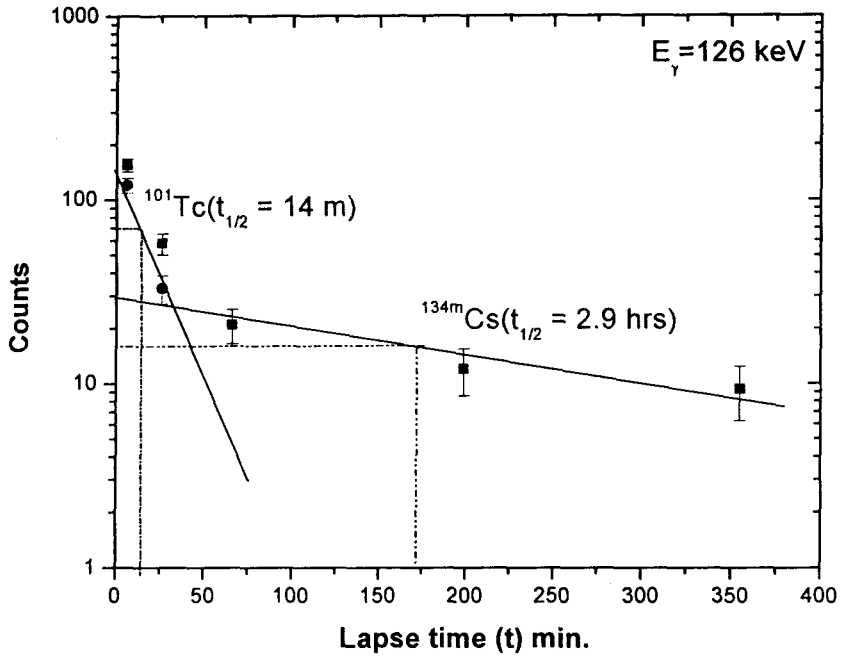

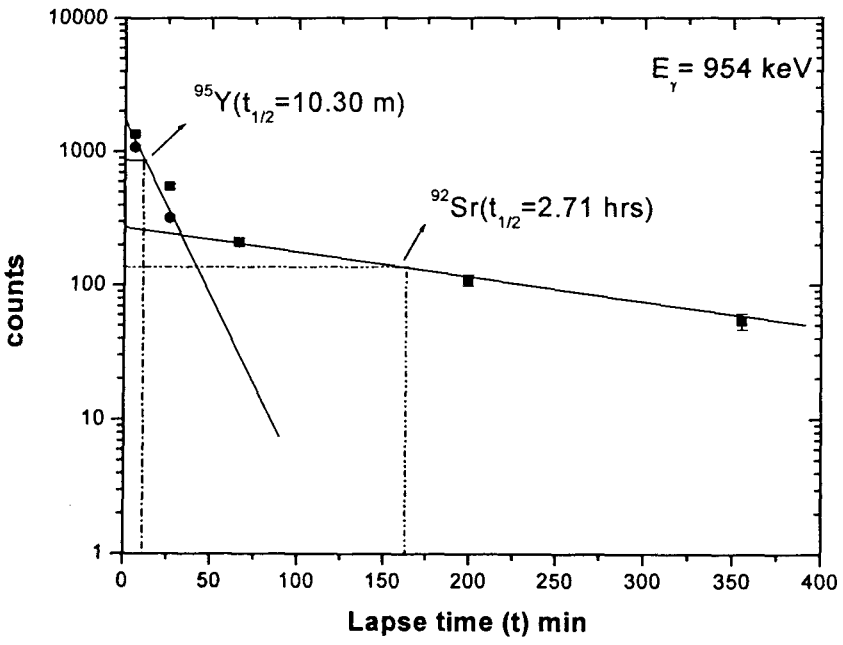

Fig.3.2.5 Typical decay curves of several residues.

Table 3.3.2 Residues which are expected to be formed via both complete fusion (CF) as well as incomplete fusion (ICF).

Residue	Reaction	half-life	γ-ray energy(keV)	branching ratio(%)
^{178}Re	$^{169}Tm(O,\alpha 3n)$	13 m	237.7	45
^{177}W	$^{169}Tm(O,\alpha p3n)$	132.6 m	115.0	59
^{178}Ta	$^{169}Tm(O,\alpha 2pn)$	147 m	325.5	94.1
^{177}Hf	$^{169}Tm(O,\alpha 3pn)$	51.4 m	638.1	20.0

Table 3.3.3 A list of residues likely to be produced by fission, their half-lives, characteristic γ-ray energy and their branching ratio.

S. No.	Residue	half-life	γ-ray energy(keV)	branching ratio(%)
1.	^{78}As	1.51 h	828.0	8.6
2.	^{131}La	59.0 m	453.7	6.4
3.	^{107}In	32.4 m	204.9	48
4.	^{66}Ge	2.26 h	108.8	10.5
5.	^{88}Nb	14.3 m	399.6	31
6.	^{95}Y	10.3 m	954.1	19
7.	^{83}Se	22.3 m	225.2	31.9
8.	^{134m}Cs	2.9 h	127.4	12.7
9.	^{123m}Sn	40.0 m	160.3	85.6
10.	^{105}Ag	7.2 m	319.2	0.9
11.	^{123}Xe	2.08 h	330.1	8.6

S. No.	Residue	half-life	γ-ray energy (keV)	branching ratio(%)
12.	^{109}Sn	18.0 m	331.0	9.7
13.	^{101}Ag	11.1 m	667.3	9.7
14.	^{79}As	9.0 m	432.0	1.50
15.	^{105}In	5.0 m	131.4	100
16.	^{108b}Rh	6.0 m	433.9	43
17.	^{95}Ru	1.64 h	806.4	4.09
18.	^{75}Br	1.62 h	427.8	4.5
19.	^{92}Y	3.54 h	448.5	2.34
20.	^{105}Tc	7.7 m	107.9	9.6
21.	^{98m}Nb	51.3 m	787.3	93
22.	^{87}Kr	1.27 h	402.6	49.6
23.	^{92}Sr	2.71 h	953.4	3.6
24.	^{101}Tc	14.0 m	127.2	2.86
25.	^{78}Ge	1.4 h	293.9	4
26.	^{137}Pr	1.28 h	160.4	0.97
27.	^{105}Ru	4.4 h	316.4	11
28.	^{104}Tc	18.0 m	358.0	79
29.	^{115a}Ag	20.0 m	131.4	2.9
30.	^{70}As	52.6 m	668.1	21.2
31.	^{127}Sn	2.1 h	805.8	8.2
32.	^{108m}In	58.0 m	242.7	38
33.	^{96}Rh	9.6 m	932.7	100
34.	^{65}Ni	2.51 h	1115.0	14.8

3.5 Measured production cross-sections

As disscused earlier the intensity of characteristic γ-rays have been used to measure the production cross-section of different residues. Measured cross-section of five different residues populated via CF channel at different incident energies are presented in Table-3.5.1. Similarly, in Table-3.5.2., are presented the measured cross-sections for four residues which are expected to be formed via CF as well as ICF. The first column in these tables lists the incident beam energy on different sample of the stack. In Table-3.5.3., the measured production cross-sections for a large number residues expected to be formed via fission of excited nuclei produced through different channels at $\approx$ 95 MeV beam energy, are given.

Table 3.5.1 Measured cross-sections for the residues formed via complete fusion(CF)

Lab. Energy (MeV)	^{181}Ir (mb)	^{181}Os (mb)	^{179}Os (mb)	^{182}Ir (mb)	^{178}Lu (mb)
71.7±1.0	5.6±1.0	9.3±1.2	38.9±2.6	-	48.0±3.2
78.7±0.9	12.5±2.3	73.1±2.4	93.0±3.8	26.4±6.4	197.3±9.1
82.0±0.8	29.3±1.7	146.2±6.1	129.3±10.0	77.3±1.7	358.0±28.0
88.9±1.0	46.3±3.2	263.2±9.5	74.2±6.3	29.2±3.2	279.0±3.7
94.6±0.4	32.5±2.6	167.3±11.2	46.1±2.6	12.6±1.2	233.2±12.6

Table 3.5.2 Measured cross-sections for the residues formed via both CF as well as ICF.

Lab. Energy (MeV)	^{178}Re (mb)	^{177}W (mb)	^{178}Ta (mb)	^{177}Hf (mb)
71.7±1.0	-	9.7±2.5	9.3±1.3	12.5±0.78
78.7±0.9	8.2±2.2	17.5±1.8	36.0±1.2	28.4±2.6
82.0±0.8	19.2±3.6	41.3±5.3	87.1±6.7	67.8±7.3
88.9±1.0	31.6±1.3	73.2±6.2	143.7±3.4	127.9±9.1
94.6±0.4	39.6±4.3	96.4±3.5	194.2±6.9	163.0±5.3

Table 3.5.3 Measured production cross-sections for fission residues at ≈95 MeV ^{16}O beam.

S. No.	Residues	cross-sections(mb)	S. No.	Residues	cross-section(mb)
1.	^{78}As	550.63±11.21	9.	^{123m}Sn	6.33±0.97
2.	^{131}La	27.26±3.24	10.	^{105}Ag	146.48±6.89
3.	^{107}In	9.46±1.65	11.	^{123}Xe	2.88±0.21
4.	^{66}Ge	3.45±0.69	12.	^{109}Sn	29.48±2.58
5.	^{88}Nb	26.01±3.78	13.	^{101}Ag	79.64±3.44
6.	^{95}Y	58.11±3.46	14.	^{79}As	375.40±12.99
7.	^{83}Se	11.73±2.19	15.	^{105}In	4.68±1.07
8.	^{134m}Cs	6.10±1.02	16.	^{108b}Rh	20.19±1.57

S. No.	Residues	cross-sections(mb)	S. No.	Residues	cross-section(mb)
17.	^{95}Ru	383.21±5.61	18.	^{75}Br	131.83±9.37
19.	^{92}Y	30.90±3.46	20.	^{105}Tc	276.22±6.86
21.	^{98m}Nb	13.39±1.41	22.	^{87}Kr	1.82±0.13
23.	^{92}Sr	128.71±4.62	24.	^{101}Tc	74.25±7.24
25.	^{78}Ge	33.21±4.19	26.	^{137}Pr	103.50±7.13
27.	^{105}Ru	36.69±2.17	28.	^{104}Tc	7.88±1.31
29.	^{115a}Ag	548.83±19.87	30.	^{70}As	33.75±1.34
31.	^{127}Sn	175.20±9.16	32.	^{108m}In	60.47±1.88
33.	^{96}Rh	25.52±1.59	34.	^{65}Ni	22.82±3.28

The residues formed through complete fusion (CF) and/or incomplete fusion (ICF) channels are discussed separately and the variations of cross-section as a function of projectile energy are also shown in the next chapter.

References

[1] Manoj Kumar Sharma, Ph. D. Thesis(2002), Aligarh Muslim University, Aligarh, India.

[2] B. P. Singh, H. D. Bhardwaj, and R. Prasad, II Nuovo Cimento, 104 A (1991) 475.

[3] B. P. Singh, Ph. D. Thesis(1991), Aigarh Muslim University, Aligarh, India.

[4] E. Browne and R. B. Firestone, Table of isotopes, Wiley, New York, 1986.

[5] Jagdish K. Tuli, Nuclear Wallet Cards, National Nuclear Data Center, Upton, New York, 2000.

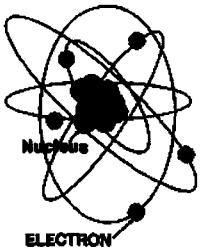

④Results and discussion

In the present work the excitation functions(EFs) for the production of several residues have been measured in the energy range $\approx$ 70-95 MeV. The residues which have been identified are expected to be formed due to several reaction channels[1, 2, 3]. Some of the possible and dominant channels may be, the residues which are produced via CF of projectile ^{16}O, with the target nucleus ^{169}Tm leading to the formation of excited composite system followed by particle emission. Some of the residues produced through complete fusion(CF) for which cross-sections are measured in the present work are ^{181}Ir, ^{182}Ir, ^{181}Os, ^{179}Os and ^{178}Lu.

The details of individual reaction channels are given below,

4.1 Complete Fusion Channels

1. $^{169}Tm(^{16}O, 3n)$ **channel** [residue = ^{182}Ir, $t_{1/2}$ = 15.0 m, J^{π} = (5)+]

   The evaporation residue ^{182}Ir is expected to be formed via complete fusion of ^{16}O with ^{169}Tm followed by the evaporation of three neutrons from the excited composite system ^{185}Ir. The EFs for this reaction is given in Fig.4.1.1(a). From this figure, it can be observed that the cross-section increases with the increase in energy and attains a maximum, after which the cross-section falls off with the increase in the energy as the other channels open-up.

2. $^{169}Tm(^{16}O, 4n)$ **channel** [residue = ^{181}Ir, $t_{1/2}$ = 5.0 m, J^{π} = (5/2)-]

   The evaporation residue ^{181}Ir is expected to be formed via complete fusion of ^{16}O with ^{169}Tm followed by the evaporation of four neutrons

from the excited composite system ^{185}Ir. The variation of cross-sections with energy for this channel is shown in Fig.4.1.1(b).

3. $^{169}Tm(^{16}O, p3n)$ **channel** [residue = ^{181}Os, $t_{1/2}$ = 105 m, J^{π} = (1/2)-]

   The evaporation residue ^{181}Os is expected to be formed via complete fusion of ^{16}O with ^{169}Tm followed by the evaporation of a proton and three neutrons from the excited composite system ^{185}Ir. The residual nucleus ^{181}Os may also be populated by the β^+ decay of its higher charge isobar precursor ^{181}Ir formed via the reaction $^{169}Tm(O, 4n)$. Thus the measured activity of ^{181}Os will have contribution from both the independent production as well as from precursor decay. The measured EFs for this reaction is shown in Fig.4.1.2(a).

4. $^{169}Tm(^{16}O, p5n)$ **channel** [residue = ^{179}Os, $t_{1/2}$ = 6.5 m, J^{π} = (1/2)-]

   The evaporation residue ^{179}Os is expected to be formed via complete fusion of ^{16}O with ^{169}Tm followed by the evaporation of a proton and five neutrons from the excited composite system ^{185}Ir. The same residual nucleus may also be populated by the β^+ decay of its higher charge isobar precursor ^{179}Ir formed via the reaction $^{169}Tm(O, 6n)$. The experimentally measured EFs for the above channel is given in Fig.4.1.2(b).

5. $^{169}Tm(^{16}O, 6pn)$ **channel** [residue = ^{178}Lu, $t_{1/2}$ = 23.1 m, J^{π} =(1+)]

   The evaporation residue ^{178}Lu is expected to be formed via complete fusion of ^{16}O with ^{169}Tm followed by the evaporation of six protons and a neutron from the excited composite system ^{185}Ir. The EFs for this channel is given in Fig.4.1.3.

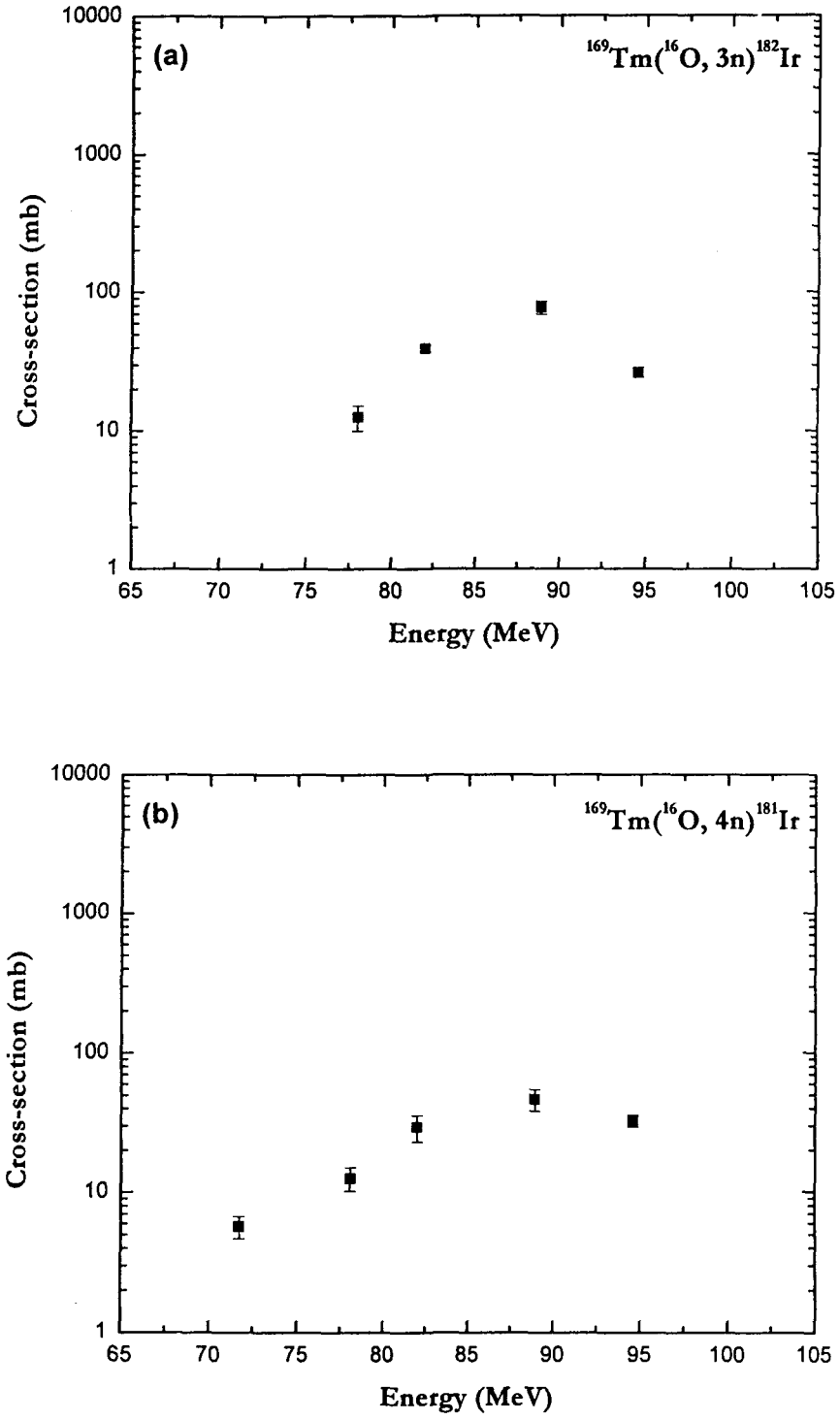

Fig.4.1.1 Experimentally measured EFs for different reaction products. .

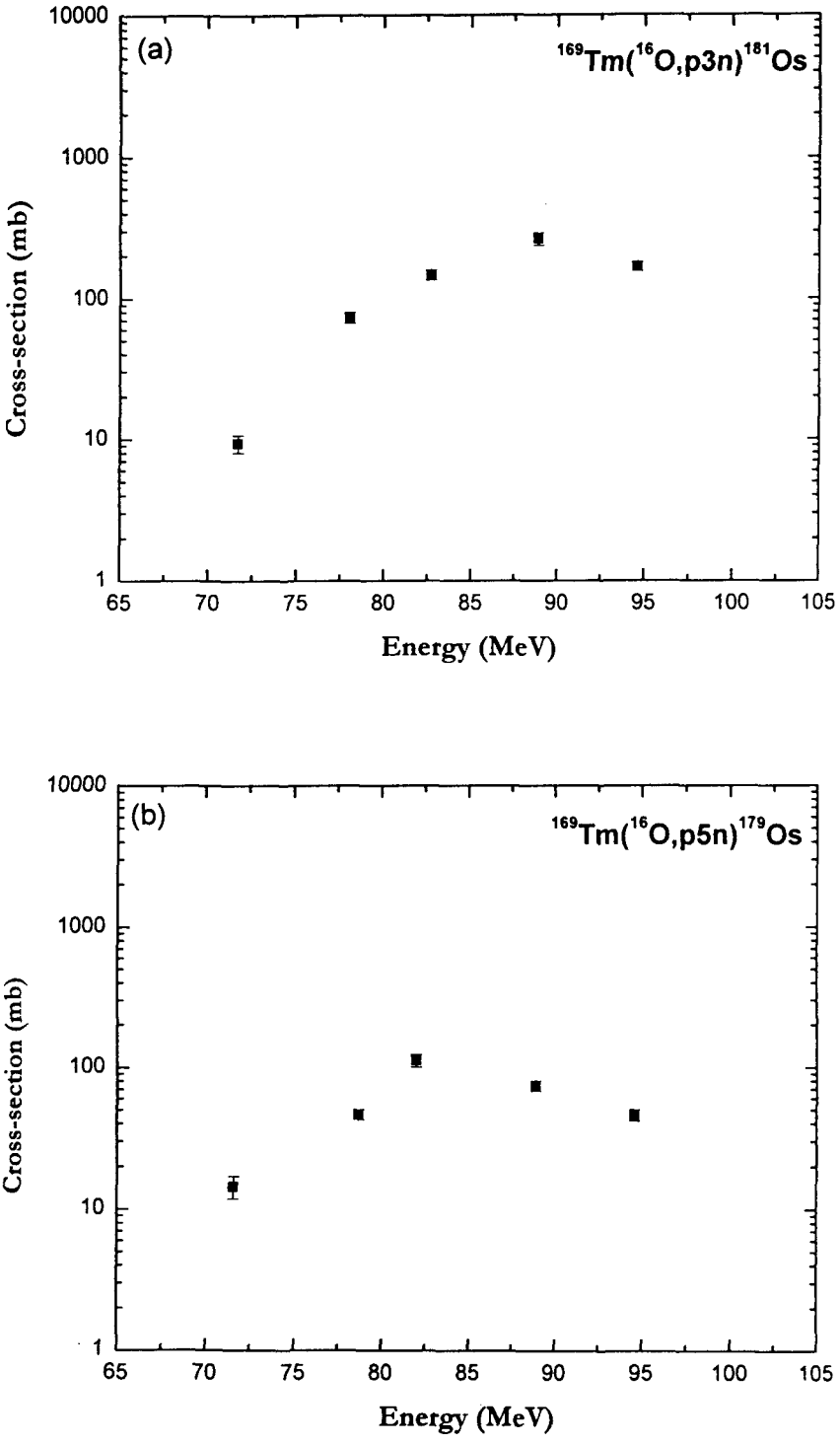

Fig.4.1.2 Experimentally measured EFs for different reaction products. .

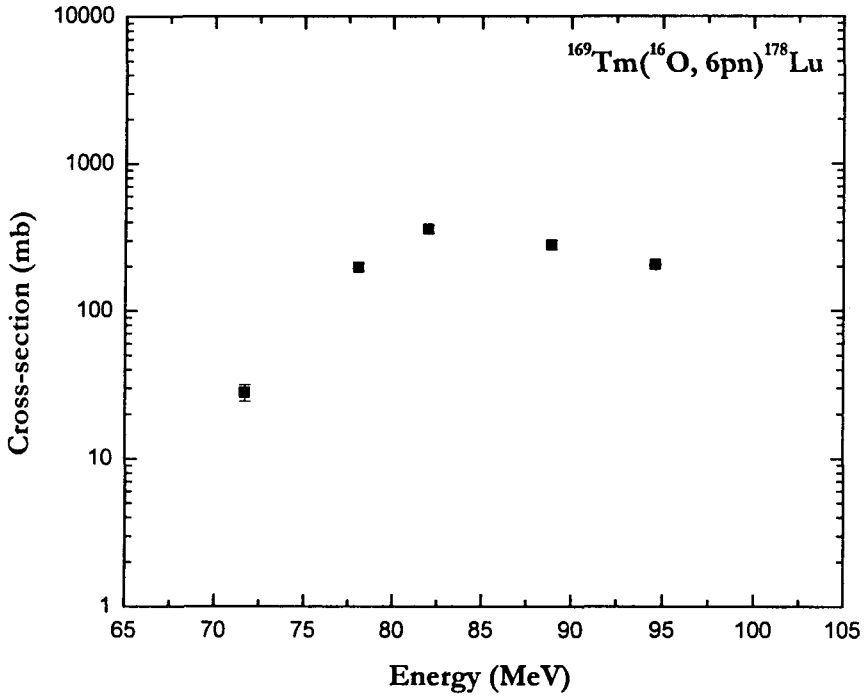

Fig.4.1.3 Experimentally measured EFs for ^{178}Lu.

Similarly, it is also possible that the composite system is formed due to the ICF, if it is assumed that the projectile ^{16}O breaks up into α and ^{12}C fragments in the presence of field of target nucleus and one of the fragments (^{12}C) fuses with the target nucleus, and unfused fragment (α-particle) moves in the forward direction with the same velocity as that of incident ion. This incomplete fusion (fusion of ^{12}C only with the target nucleus) may result into the formation of various residues by emission of different nuclear parti-

cles. Some of the identified residues produced via ICF reaction channels are ^{178}Re, ^{177}W, ^{178}Ta and ^{177}Hf. As such, the measured cross-sections for these residues may have contribution from both the CF as well as ICF channels.

The details of individual reaction channels are given below,

4.2 Incomplete Fusion Channels

1. $^{169}Tm(^{16}O, \alpha 3n)$ **channel** [residue = ^{178}Re, $t_{1/2}$ = 13.0 m, J^{π} = (3)+]

   The residue ^{178}Re may be formed by the complete fusion of ^{16}O with ^{169}Tm followed by the evaporation of an α-particle and three neutrons from excited composite system ^{185}Ir. The same residue may also be formed via incomplete fusion of ^{12}C fragment (if it is assumed that ^{16}O undergoes breakup in to α and ^{12}C fragments) followed by emission of three neutrons from excited composite system ^{181}Re and unfused fragment α-particle moves forward as a spectator as shown in Fig.4.2.1.

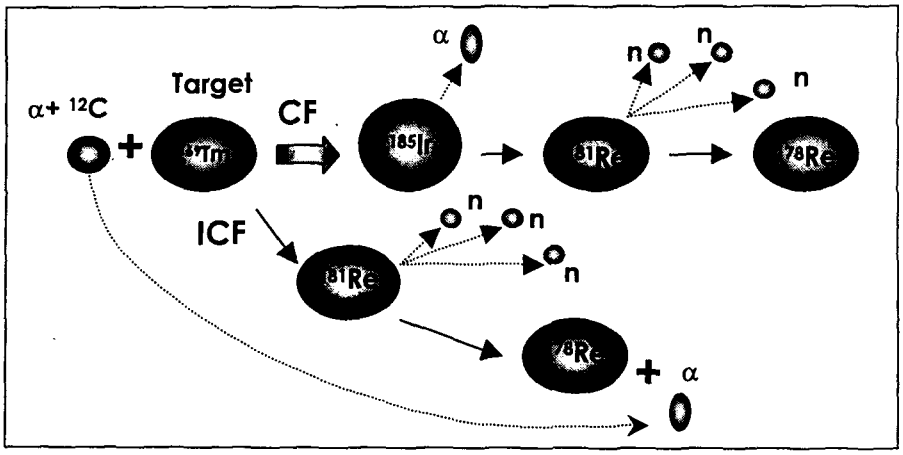

Fig.4.2.1 Pictorial representation of the production of ^{178}Re via CF as well as ICF channels.

Thus, the measured activity of ^{178}Re will have contributions from both the CF as well as ICF channels. In Fig.4.2.2 the EFs for the reaction $^{169}Tm(O, \alpha 3n)^{178}Re$ is shown.

2. $^{169}Tm(^{16}O, \alpha p3n)$ **channel** [residue = ^{177}W, $t_{1/2}$ = 132.6 m, J^{π} = (1/2)-]

   The evaporation residue ^{177}W is expected to be formed via complete fusion of ^{16}O with ^{169}Tm followed by evaporation of an α-particle, a proton and three neutrons from the excited composite system ^{185}Ir and also via incomplete fusion of ^{12}C fragment followed by emission of a proton and three neutrons from the excited composite system ^{181}Re and unfused fragment α-particle moves in forward direction as a spectator. The EFs for the production of ^{177}W is shown in Fig.4.2.3(a), which will have contribution from both Cf as well as ICF.

3. $^{169}Tm(^{16}O, \alpha 2pn)$ **channel** [residue = ^{178}Ta, $t_{1/2}$ = 147.0 m, J^{π} = (7)-]

   The evaporation residue ^{178}Ta may be formed via complete fusion of ^{16}O with ^{169}Tm followed by evaporation of an α-particle, two protons and a neutron from the excited composite system ^{185}Ir and also via incomplete fusion of ^{12}C fragment followed by emission of two protons and a neutron from the excited composite system ^{181}Re. The experimentally measured EFs for this reaction is shown in Fig.4.2.3(b).

4. $^{169}Tm(^{16}O, \alpha 3pn)$ **channel** [residue = ^{177}Hf, $t_{1/2}$ = 51.4 m, J^{π} = (7/2)-]

   The evaporation residue ^{177}Hf may be formed via complete fusion of

^{16}O with ^{169}Tm followed by evaporation of an α-particle, three protons and a neutron from the excited composite system ^{185}Ir. The same residue ^{177}Hf may also be populated via incomplete fusion of ^{12}C fragment with target nucleus ^{169}Tm followed by emission of two protons and a neutron from the excited composite system ^{181}Re. The measured EFs having the contribution from both CF and ICF channels, The variation of cross-section with energy for this reaction is shown in Fig.4.2.4.

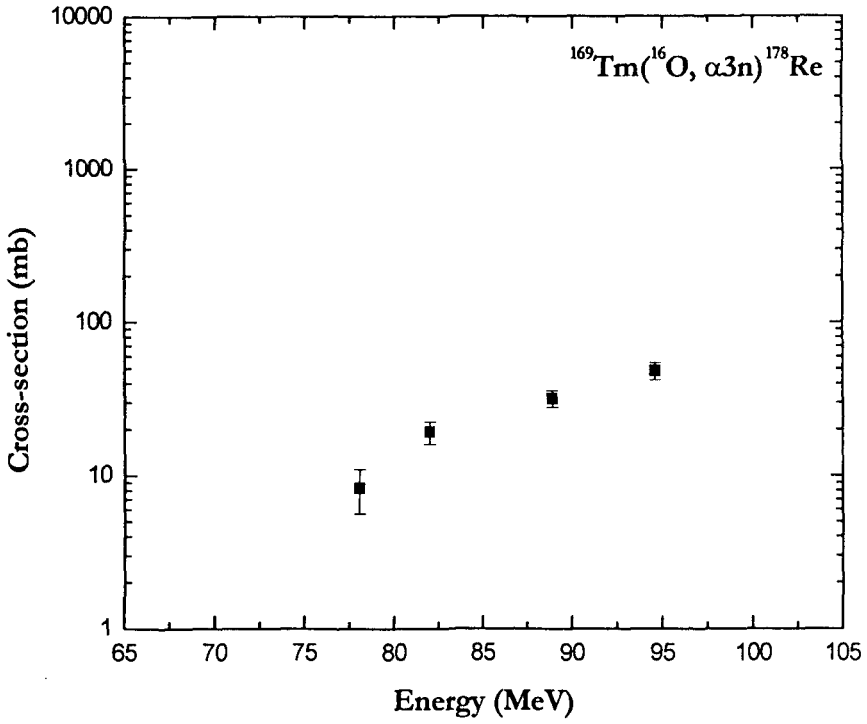

Fig.4.2.2 Experimentally measured EF for ^{178}Re reaction product.

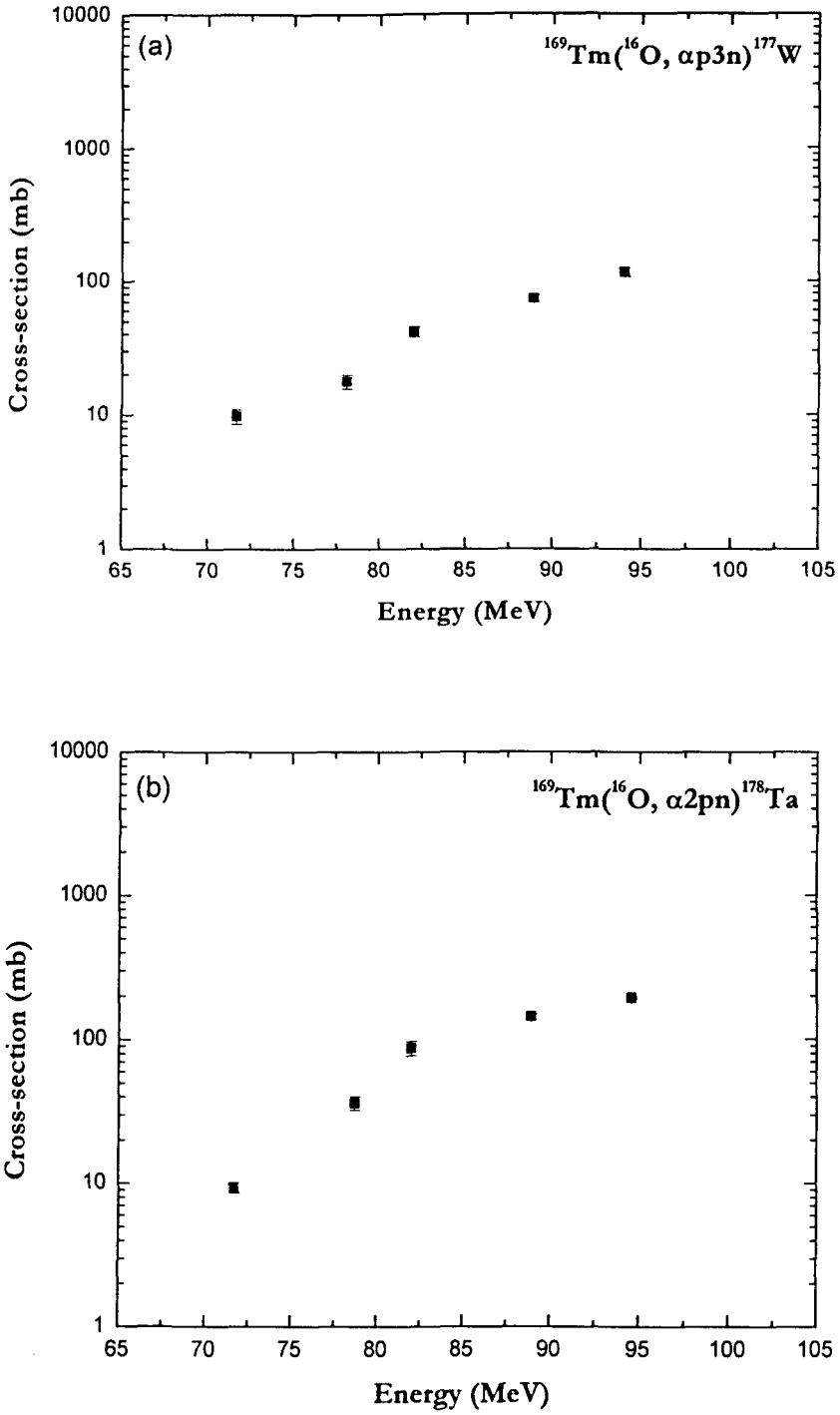

Fig.4.2.3 Experimentally measured EFs for different reaction products. .

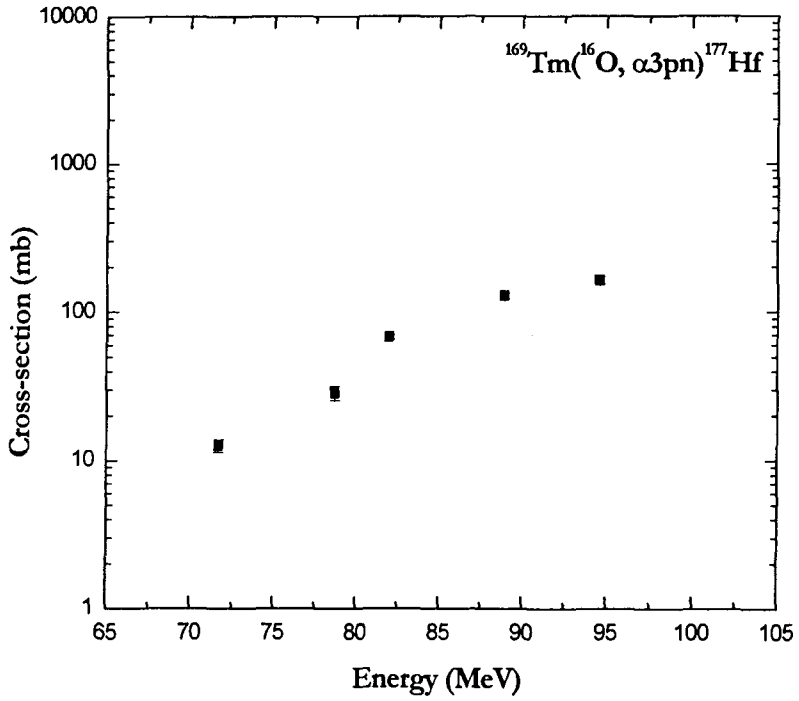

Fig.4.2.4 Experimentally measured EF for ^{177}Hf reaction product.

Further, it is also possible that the composite system formed via CF or ICF may also decay by the process of fission provided sufficient excitation energy is available[6, 7]. As already discussed, cross-sections for a large number of fission-fragments (A = 65 to 137) have also been measured at $\approx$ 95 MeV beam energy and are already given in the Table-3.5.3. A list of these fission residues is given in Table-4.1, for ready reference.

Table-4.1 List of identified fission residues

S. No.	Residues	S. No.	Residues	S. No.	Residues
1.	^{78}As	13.	^{101}Ag	25.	^{78}Ge
2.	^{131}La	14.	^{79}As	26.	^{137}Pr
3.	^{107}In	15.	^{105}In	27.	^{105}Ru
4.	^{66}Ge	16.	^{108b}Rh	28.	^{104}Tc
5.	^{88}Nb	17.	^{95}Ru	29.	^{115a}Ag
6.	^{95}Y	18.	^{75}Br	30.	^{70}As
7.	^{83}Se	19.	^{92}Y	31.	^{127}Sn
8.	^{134m}Cs	20.	^{105}Tc	32.	^{108m}In
9.	^{123m}Sn	21.	^{98m}Nb	33.	^{96}Rh
10.	^{105}Ag	22.	^{87}Kr	34.	^{65}Ni
11.	^{123}Xe	23.	^{92}Sr		
12.	^{109}Sn	24.	^{101}Tc		

These production cross-sections for these fission residues are also plotted as a function of atomic number, atomic mass number, neutron number & $(N-Z)/A$, and are shown in Figs.4.1-4.2.

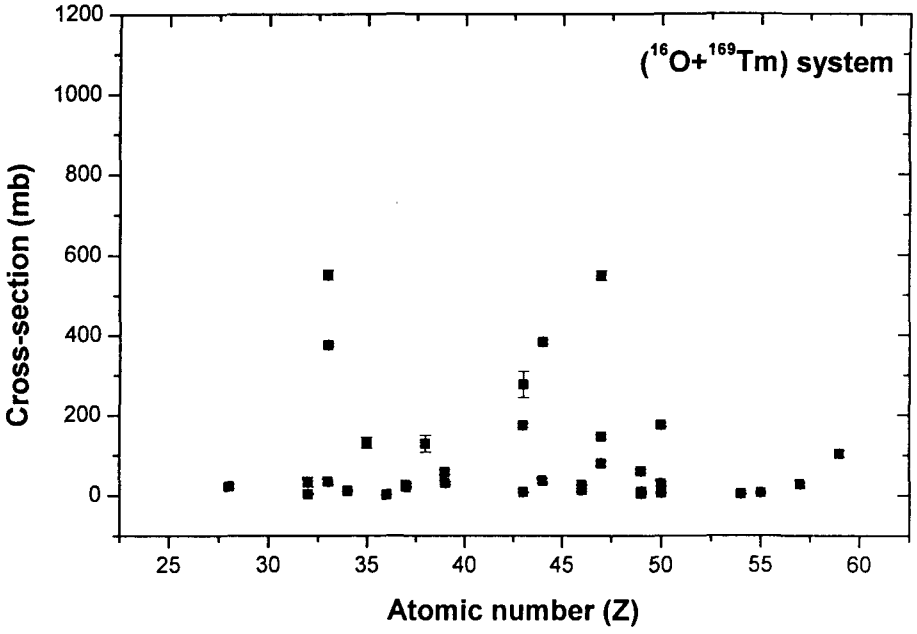

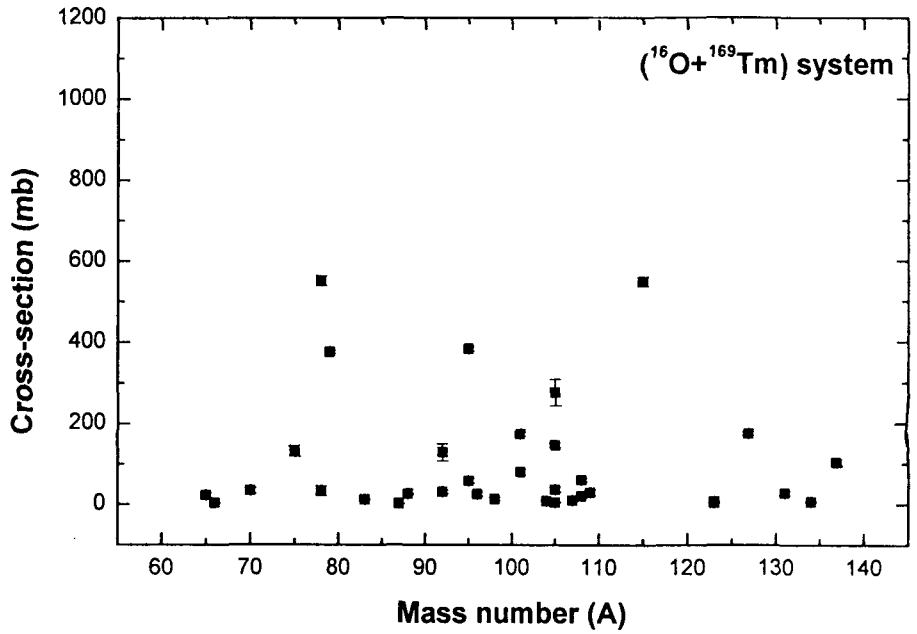

Fig.4.1 Experimentally measured cross-section of the fission residues as a function of atomic number(Z) and mass number(A).

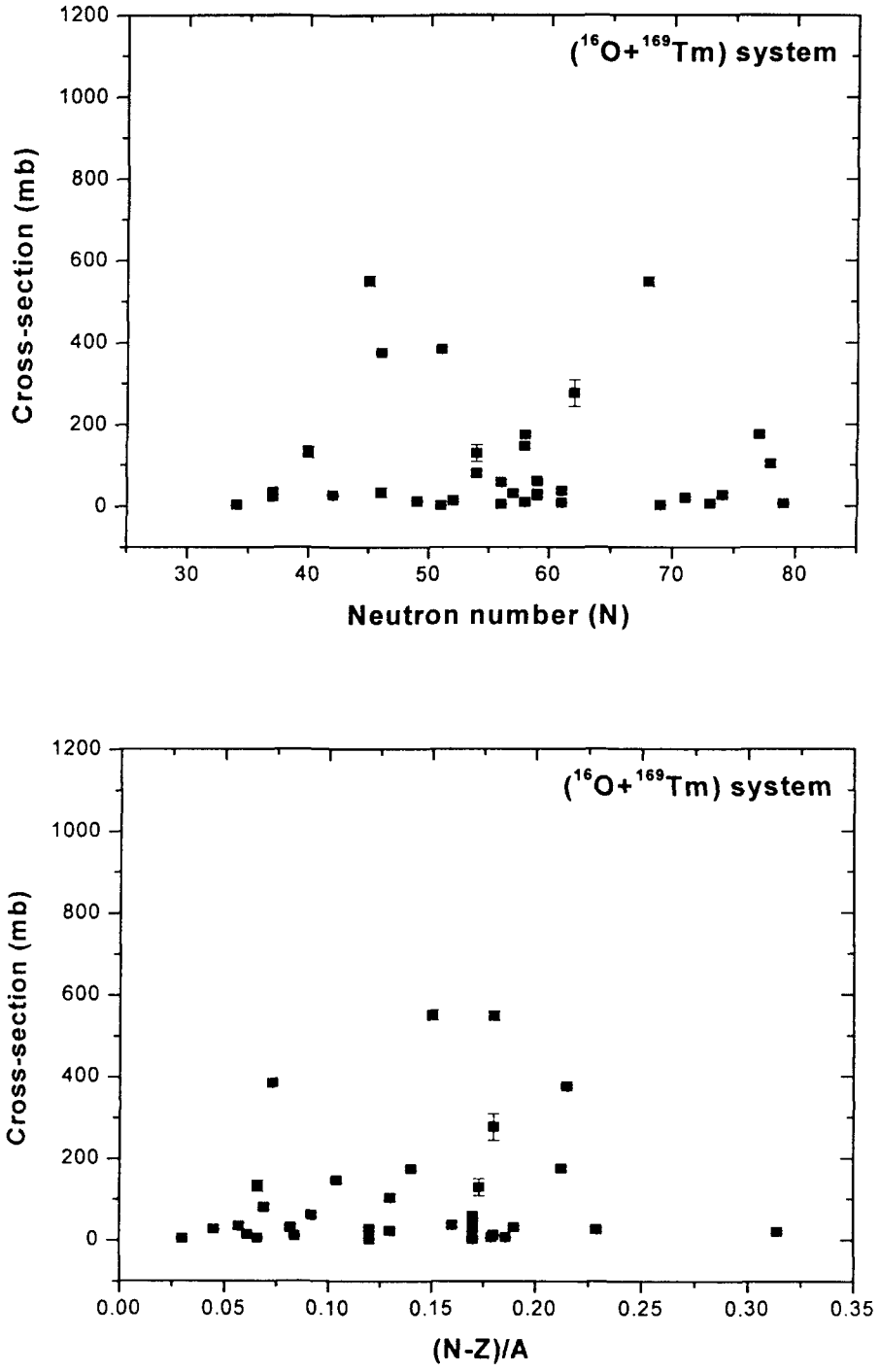

Fig.4.2 Experimentally measured cross-section of the fission residues as a function of neutron number(N) and (N-Z)/A.

In the present study, as can be seen from Figs.4.1-4.2, The mass distribution has been found to be symmetric as expected[7] at presently studied energy i.e., $E^* \approx 63$ MeV. Production cross-sections for some of the fragments are substantialy higher than expected at this energy. One of the possible reasons for the higher fission cross-section values may be the fact that the fragments which are observed in this case are populated from various decay chains and hence may have cumulative sum of cross-sections for these fragments. It may, however be mentioned that in the present work the fission fragments which recoil in the backward direction are lost and no correction for this could be applied. However, if catcher foils are put in both of the sides of the target, then both the fragments of a particular fission event in forward and backward directions may be trapped. If activities of backward and forward catcher foils are measured then symmetric mass distribution is expected. In the present work, mass and charge distributions have been studied in the fission of the neutron deficient compoud nucleus ^{185}Ir formed in $^{16}O+^{169}Tm$ system at $\approx$ 95 MeV. In order to study isotopic yield distribution of the fission fragments, the cross-section for different isotopes of As and Ag are plotted in the Fig.4.3. It may, however, be pointed out that the activities measured in forward catcher foil only were used for these isotopic yield distributions.

It may be noted that from the present analysis, it is not possible to seperate the contributions of CF and ICF channels. It is therefore, proposed to measure the recoil range distribution (RRD) of residues[4, 5] to obtain the CF and ICF contributions.

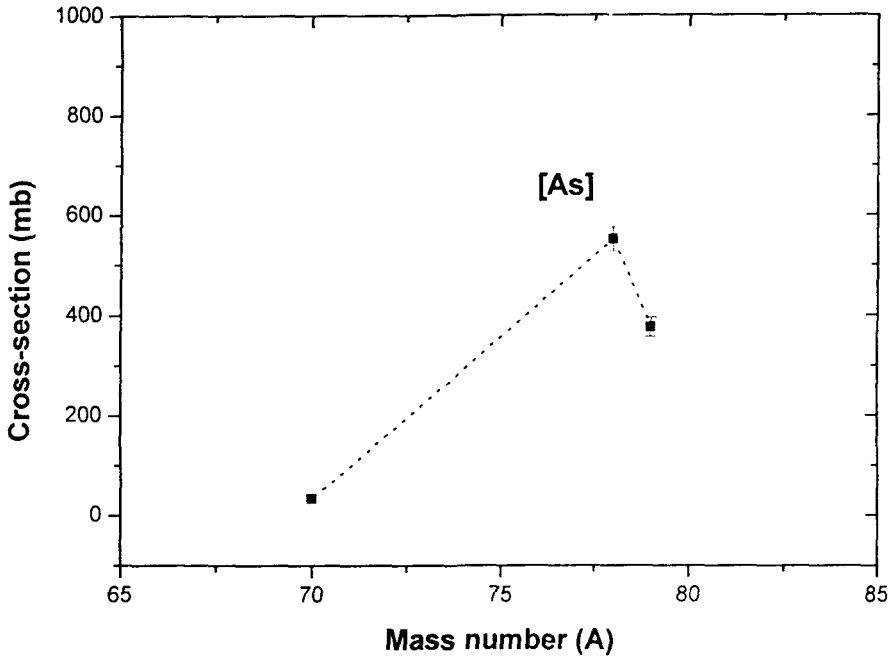

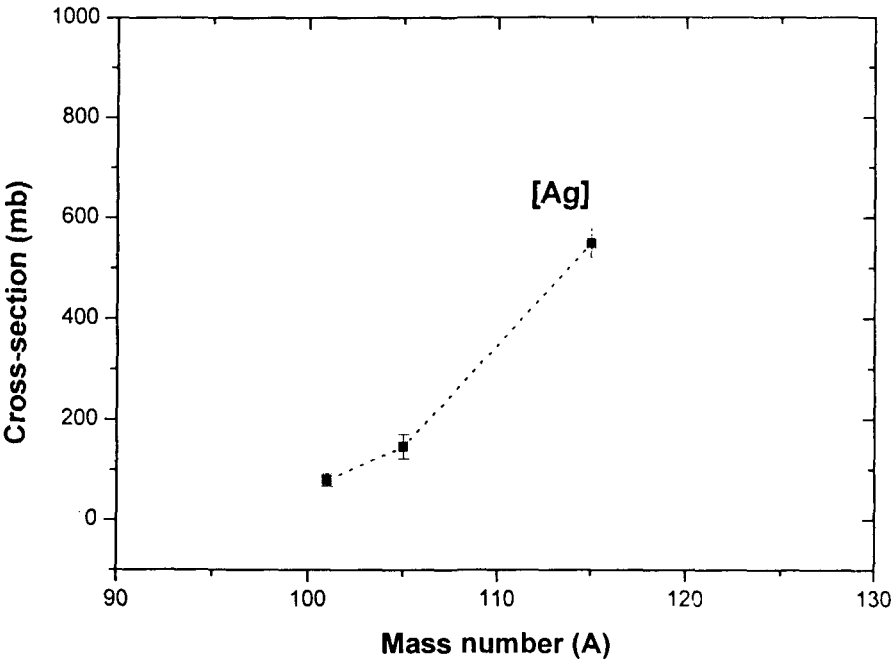

Fig.4.3 Plots of isotopic yield distribution for As and Ag isotopes.

In the present analysis it has been observed that residues are produced not only via CF and ICF channels but fission of residues produced via these channels are also important at these energies. As such, while predicting the total cross-section at medium energies, fission contribution should also be taken into consideration. It is proposed to carry out detailed measurements of fission cross-sections for several target-projectile combinations to have better understanding of the reaction processes in HI interaction.

References

[1] P. Vergani et. al., Phys. Rev. C 48(1993)1815.

[2] D. J. Parker et. al., Phys. Rev. C 44(1991)1528.

[3] B. S. Tomar et. al., Phys. Rev. C 49(1994)941.

[4] Manoj Kumar sharma et. al., Phys. Rev. C 70(2004)044606.

[5] Sunita Gupta et. al., Phys. Rev. C 61(2000)064613.

[6] E. P. Gavathas et. al., Phys. Rev. C 51(1995)1991.

[7] R. Tripathi et. al., Phys. Rev. C 69 (2004) 024613.